

# Random matrix theory of unquenched two-colour QCD with nonzero chemical potential

---

**G. Akemann,<sup>a,b</sup> T. Kanazawa,<sup>c</sup> M. J. Phillips,<sup>a</sup> and T. Wettig<sup>d</sup>**

<sup>a</sup>*Department of Mathematical Sciences & BURSt Research Centre, Brunel University West London, Uxbridge UB8 3PH, United Kingdom*

<sup>b</sup>*Department of Physics, Bielefeld University, Postfach 100131 D-33615 Bielefeld, Germany*

<sup>c</sup>*Department of Physics, University of Tokyo, Tokyo 113-0033, Japan*

<sup>d</sup>*Department of Physics, University of Regensburg, 93040 Regensburg, Germany*

*E-mail:* [akemann@physik.uni-bielefeld.de](mailto:akemann@physik.uni-bielefeld.de),  
[tkanazawa@nt.phys.s.u-tokyo.ac.jp](mailto:tkanazawa@nt.phys.s.u-tokyo.ac.jp), [michael.phillips@brunel.ac.uk](mailto:michael.phillips@brunel.ac.uk),  
[tilo.wettig@physik.uni-regensburg.de](mailto:tilo.wettig@physik.uni-regensburg.de)

**ABSTRACT:** We solve a random two-matrix model with two real asymmetric matrices whose primary purpose is to describe certain aspects of quantum chromodynamics with two colours and dynamical fermions at nonzero quark chemical potential  $\mu$ . In this symmetry class the determinant of the Dirac operator is real but not necessarily positive. Despite this sign problem the unquenched matrix model remains completely solvable and provides detailed predictions for the Dirac operator spectrum in two different physical scenarios/limits: (i) the  $\varepsilon$ -regime of chiral perturbation theory at small  $\mu$ , where  $\mu^2$  multiplied by the volume remains fixed in the infinite-volume limit and (ii) the high-density regime where a BCS gap is formed and  $\mu$  is unscaled. We give explicit examples for the complex, real, and imaginary eigenvalue densities including  $N_f = 2$  non-degenerate flavours. Whilst the limit of two degenerate masses has no sign problem and can be tested with standard lattice techniques, we analyse the severity of the sign problem for non-degenerate masses as a function of the mass split and of  $\mu$ .

On the mathematical side our new results include an analytical formula for the spectral density of real Wishart eigenvalues in the limit (i) of weak non-Hermiticity, thus completing the previous solution of the corresponding quenched model of two real asymmetric Wishart matrices.

**KEYWORDS:** Spontaneous symmetry breaking, matrix models, chiral Lagrangians, lattice QCD, real asymmetric Wishart matrices

---

## Contents

<b>1</b>	<b>Introduction</b>	<b>1</b>
<b>2</b>	<b>The partition function and two limiting theories</b>	<b>4</b>
<b>3</b>	<b>Dirac eigenvalue correlation functions</b>	<b>7</b>
3.1	Results for finite $N$	7
3.2	Eigenvalue densities at low density	10
3.3	Eigenvalue densities at high density	17
<b>4</b>	<b>The sign problem</b>	<b>21</b>
4.1	Analysis of oscillations of the Dirac spectrum	21
4.2	Average sign factor	24
4.2.1	Introductory remarks	24
4.2.2	Average sign at low density	26
4.2.3	Average sign at high density	28
<b>5</b>	<b>Conclusions</b>	<b>29</b>
<b>A</b>	<b>The weakly non-Hermitian limit of the real eigenvalue density</b>	<b>30</b>
A.1	Initial steps	30
A.2	Solution for limit of $D_N(x; \hat{\mu})$	32
A.2.1	Determination of limits of $P(j, N, \hat{\mu})$ and $D_N^+(x; \hat{\mu})$	32
A.2.2	Determination of limits of $Q(j, N, \hat{\mu})$ and $D_N^-(x; \hat{\mu})$	35
A.2.3	Final formula	36
<b>B</b>	<b>Decoupling of heavy flavours</b>	<b>36</b>
<b>C</b>	<b>Sign-quenched partition functions</b>	<b>38</b>
C.1	Main result for finite $N$	38
C.2	Proof: the $k = 1$ case	39
C.3	The large- $N$ limit of weak non-Hermiticity	39
C.4	The large- $N$ limit of strong non-Hermiticity	40

---

## 1 Introduction

The phase diagram of quantum chromodynamics (QCD) as a function of temperature  $T$  and quark chemical potential  $\mu$  is of great importance for many phenomenological questions in, e.g., heavy-ion collisions, the physics of neutron stars, and the early universe. Clearly,

nonperturbative methods are needed to study the phase diagram. Lattice QCD simulations have obtained solid quantitative results at nonzero  $T$ , see, e.g., [1], but what happens at nonzero  $\mu$  is much less well established because lattice simulations are hindered by the fermion sign problem, see [2] for a review. Some exact results could be derived for asymptotically large  $\mu$ , see, e.g., [3] for a review, but otherwise studies of the  $\mu$ -dependence of the QCD phase diagram had to rely on model approaches. Examples include the instanton liquid model [4], the PNJL model [5], and universality arguments [6]. However, there are QCD-like theories in which the fermion sign problem can be avoided for certain choices of the parameters, and which can therefore be simulated on the lattice. An example is QCD with two colours, where the single-flavour fermion determinant is real but not necessarily nonnegative so that the sign problem is absent for an even number of quark flavours whose masses are pairwise degenerate. Such theories are important testing grounds for effective theories or models since a direct comparison of analytical results with lattice data is possible. If the parameters of the theory are detuned from their “sign-free” values (e.g., if the degeneracy of the quark masses is lifted in two-colour QCD), a sign problem develops. As long as the sign problem is weak enough, one can still obtain some information from the lattice data, e.g., by reweighting, and therefore test the effective theory or model also in the presence of the sign problem. In fact, lattice studies of this kind have already been done with two-colour adjoint staggered fermions [7, 8], and we will comment on them at the end of section 4.2.2.

In this paper we will focus on two-colour QCD with  $N_f$  quark flavours in the fundamental representation of the gauge group at nonzero  $\mu$ .<sup>1</sup> This theory has been investigated in the past in great detail for both small and large  $\mu$ . For small  $\mu$ , it was studied using an effective chiral Lagrangian, see, e.g., [9], and in lattice simulations, see, e.g., [10]. One of the main results from these studies is a transition from a phase with a chiral condensate to a phase with a diquark condensate at a critical value of  $\mu$  equal to one half of the Nambu-Goldstone boson mass. For asymptotically large  $\mu$ , the physics is completely different. The ground state is believed to be a BCS superfluid of diquark pairs, for which the BCS gap has been computed in a weak-coupling approach in [11, 12]. The effective Lagrangian for this case has been derived in [13].

A very useful analytical approach to QCD and QCD-like theories is random matrix theory (RMT), which can be used either as an effective theory that yields exact results in well-defined limits, or as a schematic model to obtain qualitative results. RMT has applications in many areas of physics, see [14–21] for reviews of some of these areas. The RMT approach to QCD was pioneered in [22], and reviews can be found in [17, 23, 24]. Random matrix models for QCD at nonzero  $\mu$  have been proposed using a single random matrix [25] or two random matrices [26]. Both models describe the same physics, but the two-matrix model turns out to be easier to handle mathematically [27], due to the fact that a representation in terms of complex eigenvalues exists. Random two-matrix models were proposed for adjoint QCD at nonzero  $\mu$  [28, 29] and most recently for two-colour

---

<sup>1</sup>Most of our results apply not only to two-colour QCD but also to any QCD-like theory with pseudo-real quarks.

QCD at nonzero  $\mu$  [30], completing the set of all three chiral symmetry breaking patterns [31]. Each RMT yields exact results in the so-called microscopic regime, corresponding to the lowest order in the  $\varepsilon$ -expansion [32] of the chiral effective theory. For a comparison to lattice simulations (when these are possible) we refer to [24].

For the case of two-colour QCD, which is the topic of this paper, the random two-matrix model is explicitly given in eq. (2.1) below. It implicitly contains two parameters, see eq. (2.4). One parameter relates the random-matrix quark masses to the physical quark masses and can be identified with the low-energy constant  $G$  (in the notation of [9]) in the chiral Lagrangian. The other parameter relates the random-matrix chemical potential to the physical chemical potential and can be identified with another low-energy constant,  $F$ . Computing analytical results from RMT and matching them to lattice data then allows one to determine these two low-energy constants. It was realized in [33] that the model for two colours proposed in [30] also describes the completely different physics at large  $\mu$ , provided that the random-matrix parameter corresponding to  $\mu$  is set to a particular value which corresponds to maximal non-Hermiticity. The remaining parameter can then be identified with the BCS gap  $\Delta$ . By matching the RMT results to lattice data one could in principle determine  $\Delta$ , but it is currently unclear what computational resources are needed to go to large enough values of  $\mu$  on the lattice.

The random two-matrix model proposed in [30] was solved in [34] for  $N_f = 0$  only. The eigenvalues of the pseudo-real Dirac operator are either purely real, purely imaginary, or come in complex conjugate pairs. The spectral correlation functions of these eigenvalues were computed in the quenched case (i.e., for  $N_f = 0$ ) for finite  $N$ , where  $N$  is related to the dimension of the random matrix and assumed to be proportional to the four-volume  $V_4$ . For  $N \rightarrow \infty$  two different mathematical limits were considered, that of weak non-Hermiticity [35, 36] (corresponding to  $\mu^2 N$  finite) and that of strong non-Hermiticity (corresponding to nonzero  $\mu$  in the  $N \rightarrow \infty$  limit). In the strong non-Hermiticity limit, the microscopic spectral density was obtained for the complex, real, and imaginary eigenvalues. In the weak non-Hermiticity limit, the microscopic spectral density could only be obtained for the complex eigenvalues. In this paper, we generalise the results of [34] to nonzero  $N_f$  using the building block for finite  $N$  from [37], and we also obtain the microscopic spectral densities of the real and imaginary eigenvalues in the weak non-Hermiticity limit. Furthermore, we analyse the sign problem that arises when the quark masses are detuned for even  $N_f$  or when  $\mu$  is increased for odd  $N_f$ .<sup>2</sup> It has been argued for three colours that the sign problem and the resulting strong oscillations of the spectral density are directly responsible for the breaking of chiral symmetry in the unquenched theory [39, 40].

In the remainder of this paper, we will sometimes refer to the two mathematical limits of weak and strong non-Hermiticity as “low density” and “high density”, respectively, with the understanding that by “low density” we mean the physical regime in which  $\mu^2 F^2 V_4$  is finite and by “high density” we mean the physical regime in which a BCS gap is formed. Our RMT results can be directly applied to lattice simulations of two-colour QCD in both

---

<sup>2</sup>The possibility of unequal chemical potentials as yet another source of the sign problem is interesting, see e.g. [38], but will not be considered in this paper.

regimes.

The structure of this paper is as follows. In section 2 we define the partition function in RMT as well as in the two limiting cases of low and high density. New Pfaffian expressions for the latter are given. Section 3 first summarises the structure of finite- $N$  results for all spectral densities, expressing the unquenched quantities in terms of the quenched ones. Subsections 3.2 and 3.3 then give the final answers for the formulas and pictures of the spectral densities at weak and strong non-Hermiticity, respectively, including the explicit examples of two degenerate and non-degenerate flavours. Section 4 is devoted to a detailed analysis of the sign problem. In subsection 4.1 we first analyse the boundary, height, and frequency of the highly oscillating region of the spectral density. In subsection 4.2 we then define an observable which measures the severity of the sign problem and compute this observable for low and high density. We conclude in section 5. The derivations of several technical details are given in three appendices: Appendix A deals with the weak limit of the quenched spectral density of real eigenvalues, in appendix B we explicitly verify the decoupling of heavy flavours, and appendix C expresses the (partially) sign-quenched partition functions in terms of known spectral densities.

## 2 The partition function and two limiting theories

In this section we briefly introduce the chiral RMT and discuss its two different regimes of applicability in the physics of two-colour QCD.

The RMT partition function at finite matrix size and fixed topology  $\nu$  is given by<sup>3</sup>

$$\mathcal{Z}_N^{(N_f, \nu)}(\mu; \{m\}) = \frac{1}{(2\pi)^{N(N+\nu)}} \int_{\mathbb{R}^{N \times (N+\nu)}} dP \int_{\mathbb{R}^{N \times (N+\nu)}} dQ \exp \left[ -\frac{1}{2} \text{Tr}(PP^T + QQ^T) \right] \times \prod_{f=1}^{N_f} \det \begin{pmatrix} m_f \mathbf{1}_N & P + \mu_f Q \\ P^T - \mu_f Q^T & m_f \mathbf{1}_{N+\nu} \end{pmatrix}. \quad (2.1)$$

Here, the rectangular matrices  $P$  and  $Q$  are each of size  $N \times (N + \nu)$  with real elements, without further symmetry restriction. The prefactor is chosen to ensure that  $\mathcal{Z}_N^{(N_f=0, \nu)} = 1$ . The parameters  $\mu_f$  and  $m_f$  denote the chemical potential and quark mass, respectively, for each flavour  $f$  in the two-matrix model. The mapping of these RMT parameters to physical parameters is given in eqs. (2.4) and (2.6) below. The RMT in eq. (2.1) was introduced in [30] as a model for two-colour QCD at nonzero chemical potential. At  $\mu = 0$  the matrix  $Q$  decouples, and the remaining one-matrix model equals the known RMT for two-colour QCD [41]. In eq. (2.1) the Dirac matrix is chosen to be Hermitian in the limit  $\mu_f \rightarrow 0$ , hence we must take the  $m_f$  to be purely imaginary in applications to lattice QCD. In [34] the above RMT was solved in the quenched case ( $N_f = 0$ ) for finite  $N$  and in two different large- $N$  limits, i.e., weak and strong non-Hermiticity as explained in section 1. In [33] the precise limits in which the above RMT matches two-colour QCD with  $\mu \neq 0$  were identified.

---

<sup>3</sup>Note that our convention for the Gaussian weight is the same as in [34, 37] but different from [33].

In the first large- $N$  limit, the microscopic limit at weak non-Hermiticity ( $w$ ), all chemical potentials are set equal ( $\mu_f = \mu$ ) and are taken to zero when  $N \rightarrow \infty$  such that the product  $N\mu^2$  remains finite. Likewise, the chiral limit is taken for all masses such that the product  $\sqrt{N}m_f$  remains finite. By integrating out the random matrices, followed by a Hubbard-Stratonovich transformation and a saddle-point approximation, it was shown in [33] that the RMT partition function (2.1) maps to the static part of the chiral Lagrangian,

$$Z_w^{(N_f, \nu)}(\mu; \{m\}) \sim \int_{\text{U}(1)} d\theta \int_{\text{SU}(2N_f)} e^{i\nu\theta} dU \exp \left[ \frac{1}{2} N \mu^2 \text{Tr} \left( U I U^T \mathcal{B}^T (U I U^T)^\dagger \mathcal{B} \right) + \sqrt{N} \text{Re Tr} (e^{i\theta/N_f} U I U^T i \mathfrak{T}^\dagger) \right], \quad (2.2)$$

which provides the dominant contribution in the  $\varepsilon$ -regime of chiral perturbation theory. Here, we have introduced the  $2N_f \times 2N_f$  matrices

$$I \equiv \begin{pmatrix} \mathbf{0} & \mathbf{1} \\ -\mathbf{1} & \mathbf{0} \end{pmatrix}, \quad \mathcal{B} \equiv \begin{pmatrix} \mathbf{1} & \mathbf{0} \\ \mathbf{0} & -\mathbf{1} \end{pmatrix}, \quad \mathfrak{T} \equiv \begin{pmatrix} \mathbf{0} & -\mathbf{t}^T \\ \mathbf{t} & \mathbf{0} \end{pmatrix}, \quad (2.3)$$

where  $\mathbf{t} \equiv \text{diag}(m_1, \dots, m_{N_f})$ ,  $\mathcal{B}$  is the baryon charge matrix, and  $\mathfrak{T}$  is the mass matrix. Comparing eq. (2.2) with the static limit of the chiral Lagrangian [9] we obtain the following mapping of RMT quantities to physical quantities,

$$\hat{\mu}^2 \equiv 2N\mu^2 = 4\mu_{\text{phys}}^2 F^2 V_4, \quad (2.4a)$$

$$\hat{m}_f \equiv 2\sqrt{N}m_f = 2m_{f,\text{phys}} G V_4 \quad (2.4b)$$

with the physical parameters  $\mu_{\text{phys}}$  and  $m_{f,\text{phys}}$ , the four-volume  $V_4$ , and the low-energy constant  $G$  (in the notation of [9]). In particular, for equal masses these can be related to the pion mass  $m_\pi$  and the low-energy constant  $F$  by  $\hat{m} = 2m_\pi^2 F^2 V_4$ , where we have used the Gell-Mann–Oakes–Renner relation. The scaling of eq. (2.4b) at small chemical potential does not come as a surprise since it also holds true for vanishing chemical potential [42].

In the second large- $N$  limit, called strong non-Hermiticity ( $s$ ) in [34], a map to a completely different regime at high density was found in [33]. In this limit the RMT chemical potential is not scaled, i.e.,  $\mu = \mathcal{O}(1)$ , and it was found for an even number  $N_f$  of flavours that

$$Z_s^{(N_f, \nu=0)}(\mu = 1; \{m\}) \sim \int_{\text{U}(1)} d\phi \int_{\text{SU}(N_f)} d\tilde{U} d\tilde{V} \exp \left[ -\frac{1}{2} \text{Re Tr} (e^{2i\phi} \mathbf{t} \tilde{U} \tilde{U}^T \mathbf{t}^T \tilde{V}^* I \tilde{V}^\dagger) \right] \quad (2.5)$$

in the sector of zero topology. Here we have to identify

$$\hat{m}_f^2 \equiv m_f^2 = \frac{3}{\pi^2} V_4 \Delta^2 m_{f,\text{phys}}^2, \quad (2.6)$$

where  $\Delta$  is the BCS gap. Note that we have  $\hat{m}_f = m_f$ , i.e., no rescaling by a power of  $N$  is necessary in this regime [34].

Whilst in [33] this mapping was found at maximal non-Hermiticity ( $\mu = 1$ ), we will show below that the same result holds for  $0 < \mu \leq 1$ , both for the partition function and

for the eigenvalue density correlation functions, subject to a trivial rescaling. We also note here that the two different limits in  $\mu$  can be formally related. By taking the limit  $\hat{\mu} \rightarrow \infty$  of the results in the weak large- $N$  limit (and suitably rescaling the eigenvalues and masses), the results in the strong limit can be recovered.

The group integrals in eqs. (2.2) and (2.5) are in general very difficult to evaluate explicitly. However, in [37] a Pfaffian expression was computed for the RMT partition function (2.1) for finite  $N$  and any number of flavours. Combined with the large- $N$  limit of the building blocks of the Pfaffian expression, the kernel from [34], and the limiting individual skew-orthogonal polynomials of even degree, we find

$$Z_{w/s}^{(N_f, \nu)}(\mu; \{\hat{m}\}) \sim \frac{(-)^{[N_f/2]}}{\Delta_{N_f}(\{\hat{m}^2\})} \begin{cases} \text{Pf}_{1 \leq f, g \leq N_f} \left[ \mathcal{K}_{w/s}(\hat{m}_f^2, \hat{m}_g^2) \right] & N_f \text{ even,} \\ \text{Pf}_{1 \leq f, g \leq N_f} \begin{bmatrix} 0 & q_w(\hat{m}_g^2) \\ -q_w(\hat{m}_f^2) & \mathcal{K}_{w/s}(\hat{m}_f^2, \hat{m}_g^2) \end{bmatrix} & N_f \text{ odd (w),} \end{cases} \quad (2.7)$$

where  $[x]$  denotes the integer part of  $x$  and the Vandermonde determinant is defined as  $\Delta_N(\{z\}) \equiv \prod_{k>l}^N (z_k - z_l)$ . Note that the limiting partition function for the strong case only exists when there is an even number of flavours. The building blocks in the weak limit ( $w$ ) are the quenched limiting kernel

$$\mathcal{K}_w(u, v) = \frac{1}{256\pi\hat{\mu}^2} \int_0^1 ds s^2 e^{-2\hat{\mu}^2 s^2} \left\{ \sqrt{u} J_{\nu+1}(s\sqrt{u}) J_{\nu}(s\sqrt{v}) - \sqrt{v} J_{\nu+1}(s\sqrt{v}) J_{\nu}(s\sqrt{u}) \right\} \quad (2.8)$$

and the limit of the quenched even skew-orthogonal polynomial  $q_N$  given in eq. (A.4),

$$\begin{aligned} q_w(z) &\equiv \lim_{N \rightarrow \infty} \frac{1}{(4N)^{\nu/2} N!} \left( \frac{z}{4N} \right)^{\nu/2} q_N \left( \frac{z}{4N} \right) \\ &= 2^{-\nu} e^{-\hat{\mu}^2/2} J_{\nu}(\sqrt{z}). \end{aligned} \quad (2.9)$$

In the strong limit ( $s$ ) we have<sup>4</sup>

$$\mathcal{K}_s(u, v) = \frac{\eta_+^3}{8\pi} (u - v) e^{-\eta_-(u+v)} I_{\nu} (2\eta_+ \sqrt{uv}), \quad (2.10)$$

where we have defined

$$\eta_{\pm} \equiv \frac{1 \pm \mu^2}{4\mu^2}. \quad (2.11)$$

These objects will also appear as building blocks in expressions for the densities of Dirac eigenvalues. They are related to the quenched kernel  $\mathcal{K}_N$  (given explicitly in eq. (A.3)) as

$$\mathcal{K}_w(u, v) = \lim_{N \rightarrow \infty} \frac{1}{(4N)^2} \left( \frac{uv}{(4N)^2} \right)^{\nu/2} \mathcal{K}_N \left( \frac{u}{4N}, \frac{v}{4N} \right) \Big|_{\hat{\mu}=\sqrt{2N}\mu \text{ fixed}}, \quad (2.12)$$

$$\mathcal{K}_s(u, v) = (uv)^{\nu/2} \lim_{N \rightarrow \infty} \mathcal{K}_N(u, v). \quad (2.13)$$

---

<sup>4</sup>In order to emphasise the similarities between the weak and strong case, we have incorporated (by convention) an extra factor of  $(uv)^{\nu/2}$  into the limiting strong kernel  $\mathcal{K}_s$  compared with [34]. Corresponding factors have been removed from the limiting weight functions in eqs. (3.31) and (3.36) below. All observables remain unaffected by this choice.

We also note that the building blocks are directly related to the one- and two-flavour partition functions,

$$Z_{w/s}^{(N_f=2,\nu)}(\hat{\mu}; \hat{m}_1, \hat{m}_2) \sim \frac{\mathcal{K}_{w/s}(\hat{m}_1^2, \hat{m}_2^2)}{\hat{m}_1^2 - \hat{m}_2^2}, \quad (2.14)$$

$$Z_w^{(N_f=1,\nu)}(\hat{\mu}; \hat{m}) \sim q_w(\hat{m}^2). \quad (2.15)$$

From the explicit knowledge of the partition functions above one could in principle derive detailed sum rules for the Dirac operator eigenvalues, as was suggested in [13, 43]. However, we will be able to give more detailed unquenched density correlation functions in the following section, from which such sum rules also follow.

### 3 Dirac eigenvalue correlation functions

#### 3.1 Results for finite $N$

In the following we will be interested in finding the correlations of the eigenvalues of the Dirac operator. Within RMT this operator is given by the matrix

$$\mathcal{D}(\mu) \equiv \begin{pmatrix} \mathbf{0}_N & P + \mu Q \\ P^T - \mu Q^T & \mathbf{0}_{N+\nu} \end{pmatrix} \equiv \begin{pmatrix} \mathbf{0}_N & A \\ B^T & \mathbf{0}_{N+\nu} \end{pmatrix}, \quad (3.1)$$

with the Gaussian weights specified in eq. (2.1). In our convention, the Dirac operator is symmetric at  $\mu = 0$ , with the eigenvalues lying on the real axis. Since the Dirac operator in Euclidean field theory is actually anti-symmetric, it is necessary to multiply all eigenvalues by  $i$  when mapping from RMT to QCD.

Finding the spectrum is equivalent to finding the eigenvalues  $\Lambda_j^2$  of the Wishart matrix  $AB^T$ , as can be seen from the characteristic equation

$$0 = \det[\Lambda \mathbf{1}_{2N+\nu} - \mathcal{D}(\mu)] = \Lambda^\nu \det[\Lambda^2 \mathbf{1}_N - AB^T] = \Lambda^\nu \prod_{j=1}^N (\Lambda^2 - \Lambda_j^2). \quad (3.2)$$

Because the matrix elements of  $A$  and  $B$  are real the solutions of the characteristic equation in  $\Lambda^2$  are either real or come in complex conjugate pairs. Consequently the determinant of the Dirac operator is always real, but not necessarily positive. Hence, for two-colour QCD there is no phase problem but a true sign problem.

Switching back from Wishart to Dirac eigenvalues  $\Lambda_j$  we therefore have three possibilities: The  $\Lambda_j$  can be real ( $\Lambda_j^2 > 0$ ), imaginary ( $\Lambda_j^2 < 0$ ), or come in complex quadruplets ( $\pm\Lambda_j, \pm\Lambda_j^*$ ). In addition there are generically  $\nu$  eigenvalues equal to zero.

For simplicity we will assume that  $N = 2n$  is even. Because we will subsequently take the large- $N$  limit this is not important.<sup>5</sup> The partition function (2.1) can be expressed in

---

<sup>5</sup>Results for odd  $N$  are also known, and it is expected that they will lead to the same large- $N$  spectral densities.

terms of the Wishart eigenvalues  $z_j \equiv \Lambda_j^2$ , and the most compact form derived in [37] reads

$$\begin{aligned} \mathcal{Z}_N^{(N_f, \nu)}(\mu; \{m\}) &\equiv \prod_{k=1}^N \int_{\mathbb{C}} d^2 z_k P_N^{(N_f)}(z_1, \dots, z_N) \\ &\sim \prod_{f=1}^{N_f} m_f^\nu \prod_{k=1}^N \int_{\mathbb{C}} d^2 z_k \prod_{j=1}^{N/2} F^{(N_f)}(z_{2j-1}, z_{2j}) \Delta_N(\{z\}), \end{aligned} \quad (3.3)$$

where in the second line we have ordered the eigenvalues. This is achieved by the anti-symmetric bi-variate weight function defined as

$$\begin{aligned} F^{(N_f)}(z_1, z_2) &\equiv \prod_{f=1}^{N_f} (z_1 - m_f^2)(z_2 - m_f^2) \left\{ 2i g(z_1, z_2) [\Theta(\text{Im } z_1) - \Theta(\text{Im } z_2)] \delta^2(z_2 - z_1^*) \right. \\ &\quad \left. + h(z_1)h(z_2) \delta(\text{Im } z_1) \delta(\text{Im } z_2) \text{sgn}(\text{Re } z_2 - \text{Re } z_1) \right\}. \end{aligned} \quad (3.4)$$

In contrast to [37] we have made the mass terms explicit in  $F^{(N_f)}$ . It contains the quenched weight functions

$$\begin{aligned} h(z) &\equiv 2|z|^{\nu/2} e^{\eta_- z} K_{\frac{\nu}{2}}(\eta_+ |z|), \quad (3.5) \\ g(z_1, z_2) &\equiv 2|z_1 z_2|^{\nu/2} e^{\eta_-(z_1+z_2)} \int_0^\infty \frac{dt}{t} e^{-\eta_+^2 t(z_1^2+z_2^2)-1/4t} K_{\frac{\nu}{2}}(2\eta_+^2 t z_1 z_2) \text{erfc}\left(\eta_+ \sqrt{t} |z_2 - z_1|\right), \end{aligned} \quad (3.6)$$

where  $K$  and  $\text{erfc}$  denote the modified Bessel function of the second kind and the complementary error function, respectively. We note that in the limit of real arguments  $x$ ,  $\lim_{z_{1,2} \rightarrow x} g(z_1, z_2) = h(x)^2$ .

We are now able to give the result for all density correlation functions. The  $k$ -point density correlation function for Wishart eigenvalues is defined in the standard way. For finite (and even)  $N$ , it reads

$$\begin{aligned} R_k^{(N_f)}(z_1, \dots, z_k) &\equiv \frac{N!}{(N-k)!} \frac{1}{\mathcal{Z}_N^{(N_f, \nu)}(\mu; \{m\})} \int_{\mathbb{C}} d^2 z_{k+1} \cdots \int_{\mathbb{C}} d^2 z_N P_N^{(N_f)}(\{z\}) \\ &= \text{Pf}_{1 \leq i, j \leq k} \begin{bmatrix} \mathcal{K}_N^{(N_f)}(z_i, z_j) & \int_{\mathbb{C}} d^2 z \mathcal{K}_N^{(N_f)}(z_i, z) F^{(N_f)}(z, z_j) \\ - \int_{\mathbb{C}} d^2 z \mathcal{K}_N^{(N_f)}(z_j, z) F^{(N_f)}(z, z_i) & F^{(N_f)}(z_i, z_j) - \int_{\mathbb{C}} d^2 z F^{(N_f)}(z_i, z) \\ & \times \int_{\mathbb{C}} d^2 z' \mathcal{K}_N^{(N_f)}(z, z') F^{(N_f)}(z', z_j) \end{bmatrix}. \end{aligned} \quad (3.7)$$

It is given by a Pfaffian of the ordinary,  $2k \times 2k$  matrix composed of the matrices inside the square brackets, containing the unquenched kernel  $\mathcal{K}_N^{(N_f)}(u, v)$  and single or double integrals folded with the anti-symmetric weight function  $F^{(N_f)}(u, v)$  from eq. (3.4). Thus for fixed  $k$  there will be various contributions to  $R_k^{(N_f)}$ , beginning with one having only  $k$

complex eigenvalues, then ranging over all mixed possibilities, to one having only  $k$  real eigenvalues.

The unquenched kernel can be expressed as follows [37] in terms of the quenched kernel  $\mathcal{K}_N$  (given explicitly in eq. (A.3)) at finite (and even)  $N$ ,

$$\mathcal{K}_N^{(N_f)}(u, z) = \frac{\text{Pf} \begin{bmatrix} 0 & \mathcal{K}_{N+N_f}(u, z) & \mathcal{K}_{N+N_f}(u, m_g^2) \\ \mathcal{K}_{N+N_f}(z, u) & 0 & \mathcal{K}_{N+N_f}(z, m_g^2) \\ \mathcal{K}_{N+N_f}(m_f^2, u) & \mathcal{K}_{N+N_f}(m_f^2, z) & \mathcal{K}_{N+N_f}(m_f^2, m_g^2) \end{bmatrix}}{\prod_{f=1}^{N_f} (u - m_f^2)(z - m_f^2) \text{Pf} [\mathcal{K}_{N+N_f}(m_f^2, m_g^2)]}. \quad (3.8)$$

This expression is valid for an even number  $N_f$  of flavours, and even  $N$ . A similar expression holds for odd  $N_f$  as given in eq. (5.32) in [37] and also includes skew-orthogonal polynomials of even degree, as given in eq. (A.4) (cf. eqs. (3.25) and (3.26) for  $N_f = 1$  as an example). Because of eq. (2.7) the unquenched kernel can also be written as the ratio of two partition functions, for both even and odd  $N_f$ .

Let us also comment on the two different large- $N$  limits that can be obtained from eqs. (3.7) and (3.8). In the strong limit for an even number of flavours, all  $k$ -point correlation functions follow unambiguously by replacing the kernels in eq. (3.8) with the one in the strong limit, eq. (2.10). At weak non-Hermiticity the large- $N$  limit is more involved, as was already noted in [34], due to the non-interchangeability of the limit and the integration.<sup>6</sup> Considering only complex eigenvalues this is not an issue as all integrations are “killed” by the delta functions in  $F^{(N_f)}$  from eq. (3.4), and the  $k$ -point densities follow by using the kernel in the weak limit, eq. (2.8), in eq. (3.8). Once correlations of real Wishart eigenvalues are computed the non-interchangeability becomes significant, as is explained for the quenched building blocks in appendix A. For the spectral density of real eigenvalues we explicitly evaluate the limiting expressions for  $N_f = 0, 1, 2$ , and then a higher number of flavours readily follows. Higher  $k$ -point correlation functions in the weak limit that contain real eigenvalues will also involve double integrals (see the lower right block in the Pfaffian (3.7)) which may require further analysis.

Although the structure of the most general  $k$ -point function with arbitrary  $N_f$  is clear from the results above, in the following we will focus mainly on the most useful examples, that is, the spectral densities of complex, real, and imaginary Dirac eigenvalues with few (or no) flavours. They can be obtained from the spectral density (i.e., the one-point function) of the Wishart eigenvalues, which follows from a single kernel and is given by

$$R_1^{(N_f)}(z_1) = \int_{\mathbb{C}} d^2 z \mathcal{K}_N^{(N_f)}(z_1, z) F^{(N_f)}(z, z_1) \equiv R_1^{(N_f, \mathbb{C})}(z_1) + \delta(y_1) R_1^{(N_f, \mathbb{R})}(x_1), \quad (3.9)$$

where we denoted  $z_1 = x_1 + iy_1$ . The delta functions in the first and second line of  $F^{(N_f)}$  in eq. (3.4) lead to the split into separate densities of complex and real Wishart eigenvalues.

<sup>6</sup>This fact has nothing to do with the sign problem as it also occurs at  $\mu = 0$  [41].

The densities of complex, real, and imaginary Dirac eigenvalues are then obtained from

$$\begin{aligned}\rho_1^{(N_f, \mathbb{C})}(z) &= 4|z|^2 R_1^{(N_f, \mathbb{C})}(z^2), \\ \rho_1^{(N_f, \mathbb{R})}(x) &= 2|x| R_1^{(N_f, \mathbb{R})}(x^2), \\ \rho_1^{(N_f, i\mathbb{R})}(iy) &= 2|y| R_1^{(N_f, \mathbb{R})}(-y^2).\end{aligned}\tag{3.10}$$

To clarify the difference to the non-Hermitian RMT for three-colour QCD with  $\mu \neq 0$  [26, 27] let us briefly summarise the distinctive features of the spectral density for complex Dirac eigenvalues in the present case:

- (A)  $\rho_1^{(N_f, \mathbb{C})}(z)$  has no imaginary part.
- (B)  $\rho_1^{(N_f, \mathbb{C})}(z) = \rho_1^{(N_f, \mathbb{C})}(z^*) = \rho_1^{(N_f, \mathbb{C})}(-z^*)$ .
- (C)  $\rho_1^{(N_f, \mathbb{C})}(z)$  becomes zero for real and imaginary  $z$ .

(A) and (B) follow from the reality and chiral symmetry of the Dirac determinant, while (C) is a result of the eigenvalue repulsion: If  $z$  approaches the real axis,  $z$  and  $z^*$  come close to each other, but the corresponding probability is highly suppressed by the Vandermonde determinant  $\Delta_N(\{z^2\})$  of Dirac eigenvalues, and the same statement holds for  $z$  and  $-z^*$ . (A)–(C) hold for any finite  $N$ , and as we will see also in the large- $N$  limit.

We now turn directly to the results in the two different large- $N$  limits. For some details in the quenched case, see also [37].

### 3.2 Eigenvalue densities at low density

In this subsection we give the results valid for the microscopic limit at weak non-Hermiticity ( $w$ ). In this limit we rescale the chemical potential, the masses, and the Dirac eigenvalues in the following way (see eq. (2.4)),

$$\begin{aligned}\hat{\mu}^2 &\equiv 2N\mu^2, \\ \hat{m}_f &\equiv 2\sqrt{N}m_f, \\ \xi &\equiv 2\sqrt{N}\Lambda.\end{aligned}\tag{3.11}$$

Under these scalings, and at large  $N$ , the microscopic densities for Wishart (squared) eigenvalues are given by

$$\begin{aligned}R_w^{(N_f, \mathbb{C})}(z) &\equiv \lim_{N \rightarrow \infty} \frac{1}{(4N)^2} R_1^{(N_f, \mathbb{C})}\left(\frac{z}{4N}\right), \\ R_w^{(N_f, \mathbb{R})}(x) &\equiv \lim_{N \rightarrow \infty} \frac{1}{4N} R_1^{(N_f, \mathbb{R})}\left(\frac{x}{4N}\right).\end{aligned}\tag{3.12}$$

We can then switch back to Dirac eigenvalues using the mappings in eq. (3.10). Because  $R_1^{(N_f, \mathbb{R})}(-x^2) \neq R_1^{(N_f, \mathbb{R})}(x^2)$ , i.e., the function is not symmetric in general, the densities of real and imaginary Dirac eigenvalues will also differ in general:  $\rho_w^{(N_f, \mathbb{R})}(\xi) \neq \rho_w^{(N_f, i\mathbb{R})}(i\xi)$ . Later in the strongly non-Hermitian limit a symmetry between the real and imaginary densities will emerge.

We will first give the quenched quantities. As was shown in [34] from eqs. (3.9) and (3.4) the density of complex eigenvalues is given simply by the rescaled weight function  $\hat{g}_w(\xi^{*2}, \xi^2)$  multiplied by the weak limiting kernel in eq. (2.8),

$$\rho_w^{(N_f=0, \mathbb{C})}(\xi) = 4|\xi|^2 \hat{g}_w(\xi^{*2}, \xi^2) \mathcal{K}_w(\xi^2, \xi^{*2}), \quad (3.13)$$

where

$$\begin{aligned} \hat{g}_w(z, z^*) &= -\hat{g}_w(z^*, z) \equiv 2i \operatorname{sgn}(\operatorname{Im} z) \lim_{N \rightarrow \infty} \frac{1}{(4N)^2} \left( \frac{4N}{|z|} \right)^\nu g\left(\frac{z}{4N}, \frac{z^*}{4N}\right) \\ &= 4i \operatorname{sgn}(\operatorname{Im} z) e^{\frac{1}{4\hat{\mu}^2} \operatorname{Re} z} \int_0^\infty \frac{dt}{t} e^{-\frac{t}{64\hat{\mu}^4}(z^2+z^{*2})-\frac{1}{4t}} K_{\frac{\nu}{2}}\left(\frac{t}{32\hat{\mu}^4}|z|^2\right) \operatorname{erfc}\left(\frac{\sqrt{t}}{4\hat{\mu}^2}|\operatorname{Im} z|\right). \end{aligned} \quad (3.14)$$

The weak limit of the density of real and imaginary eigenvalues is not quite so straightforward. From eqs. (3.9) and (3.4) the density of Wishart eigenvalues  $R_1^{(N_f, \mathbb{R})}(x)$  is given by a real integral over the finite- $N$  kernel. It turns out that it is not possible to exchange the limit  $N \rightarrow \infty$  with this integration, a fact that already occurs for  $\mu = 0$  and  $N_f = 0$  in [41]. In appendix A we derive the new quenched result

$$\rho_w^{(N_f=0, (i)\mathbb{R})}(\xi) = -2|\xi| G_w(\xi^2, \xi^2), \quad (3.15)$$

where

$$\begin{aligned} G_w(x, x') &\equiv -\frac{\hat{h}_w(x')}{[\operatorname{sgn}(x')]^{\nu/2}} \left\{ \left( (-i)^\nu \int_{-\infty}^0 dy + \frac{2}{[\operatorname{sgn}(x')]^{\nu/2}} \int_0^{x'} dy \right) \mathcal{K}_w(x, y) \hat{h}_w(y) \right. \\ &\quad - \frac{1}{32\sqrt{\pi}} \left[ -\frac{1}{\hat{\mu}} e^{-\hat{\mu}^2} J_\nu(\sqrt{x}) + \frac{2\hat{\mu}^\nu}{\Gamma\left(\frac{\nu+1}{2}\right)} \int_0^1 ds e^{-\hat{\mu}^2 s^2} s^{\nu+2} \right. \\ &\quad \left. \left. \times \left( \frac{\sqrt{x}}{2} E_{\frac{1-\nu}{2}}(\hat{\mu}^2 s^2) J_{\nu+1}(s\sqrt{x}) - \hat{\mu}^2 s \left( E_{\frac{-1-\nu}{2}}(\hat{\mu}^2 s^2) - E_{\frac{1-\nu}{2}}(\hat{\mu}^2 s^2) \right) J_\nu(s\sqrt{x}) \right) \right] \right\}. \end{aligned} \quad (3.16)$$

Here we have defined the rescaled real weight function

$$\hat{h}_w(x) \equiv \lim_{N \rightarrow \infty} \frac{1}{4N} \left( \frac{4N}{|x|} \right)^{\nu/2} h\left(\frac{x}{4N}\right) = e^{x/8\hat{\mu}^2} 2K_{\frac{\nu}{2}}\left(\frac{|x|}{8\hat{\mu}^2}\right) \quad (3.17)$$

and used the exponential integral, which is defined as

$$E_n(x) \equiv \int_1^\infty dt t^{-n} e^{-xt}. \quad (3.18)$$

Equation (3.15) is plotted in figures 1 and 2 for  $\hat{\mu} = \sqrt{0.2}$  and 1, each at  $\nu = 0$  and 2. We observe that the presence of exact zero modes leads to a depletion of the spectral densities near zero.

We now turn to the unquenched densities, where we will give two examples which are both new: two generic flavours ( $N_f = 2$ ), including the degenerate mass limit, and a single flavour ( $N_f = 1$ ). We start with a general remark: when expanding the Pfaffian in the numerator of the unquenched kernel in eq. (3.8), we find that it always contains the

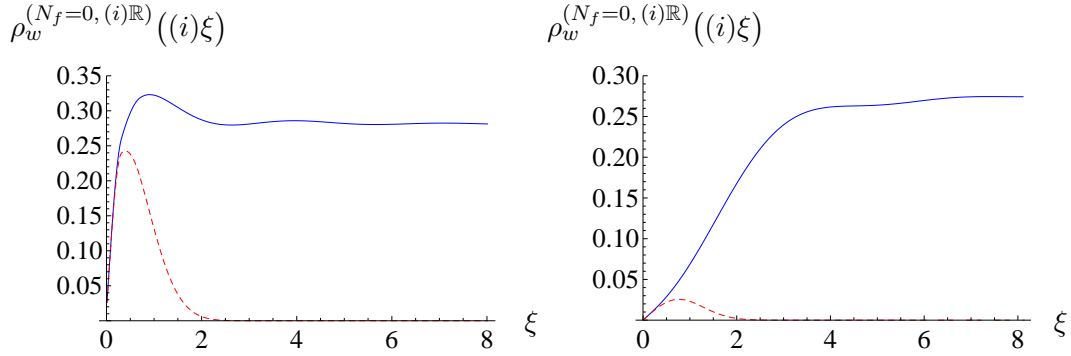


**Figure 1.** Quenched spectral density of real (blue solid line) and imaginary (red dashed line) Dirac eigenvalues on the positive half-line in the microscopic limit at weak non-Hermiticity for  $\hat{\mu} = \sqrt{0.2}$  at  $\nu = 0$  (left) and  $\nu = 2$  (right).

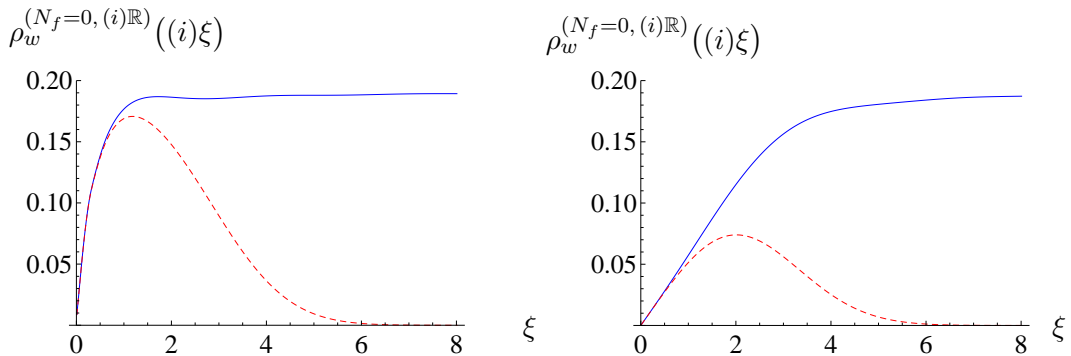


**Figure 2.** Same as figure 1 but for  $\hat{\mu} = 1$  at  $\nu = 0$  (left) and  $\nu = 2$  (right).

quenched kernel  $\mathcal{K}_{N+N_f}(u, v)$  times a Pfaffian  $\text{Pf}[\mathcal{K}_{N+N_f}(m_f^2, m_g^2)]$  that is the same as the Pfaffian in the denominator and hence cancels; the remaining product in the denominator is cancelled by factors in the weight function. Therefore, on inserting this into eq. (3.9), the unquenched density is seen always to be of the form of the quenched density plus a correction term,

$$R_1^{(N_f)}(z) \equiv R_1^{(N_f=0)}(z) + \Delta R_1^{(N_f)}(z), \quad (3.19)$$

for both the complex and the real Wishart eigenvalues. This argument holds for both an even and an odd number of flavours.

The two-flavour density of complex eigenvalues is therefore obtained in a straightforward manner,

$$\begin{aligned} \rho_w^{(N_f=2, \mathbb{C})}(\xi; \hat{m}_1, \hat{m}_2) &= \rho_w^{(N_f=0, \mathbb{C})}(\xi) \\ &+ 4|\xi|^2 \hat{g}_w(\xi^{*2}, \xi^2) \frac{\mathcal{K}_w(\xi^2, \hat{m}_2^2) \mathcal{K}_w(\xi^{*2}, \hat{m}_1^2) - \mathcal{K}_w(\xi^2, \hat{m}_1^2) \mathcal{K}_w(\xi^{*2}, \hat{m}_2^2)}{\mathcal{K}_w(\hat{m}_1^2, \hat{m}_2^2)}, \end{aligned} \quad (3.20)$$

with the quenched density from eq. (3.13) and the limiting weight function (3.14). It is of the same form as for the symplectic ensemble relevant for adjoint QCD [29]. In the limit of degenerate masses we simply have to Taylor-expand the ratio of quenched kernels in the

second line, where the denominator vanishes like  $\hat{m}_1 - \hat{m}_2$ . For convenience we also give the limiting expression,

$$\begin{aligned} \lim_{\hat{m}_2 \rightarrow \hat{m}_1} \frac{\mathcal{K}_w(\xi^2, \hat{m}_2^2) \mathcal{K}_w(\xi^{*2}, \hat{m}_1^2) - \mathcal{K}_w(\xi^2, \hat{m}_1^2) \mathcal{K}_w(\xi^{*2}, \hat{m}_2^2)}{\mathcal{K}_w(\hat{m}_1^2, \hat{m}_2^2)} \\ = \frac{\mathcal{D}_w(\xi^2, \hat{m}_1^2) \mathcal{K}_w(\xi^{*2}, \hat{m}_1^2) - \mathcal{K}_w(\xi^2, \hat{m}_1^2) \mathcal{D}_w(\xi^{*2}, \hat{m}_1^2)}{\mathcal{D}_w(\hat{m}_1^2, \hat{m}_1^2)}, \end{aligned} \quad (3.21)$$

where

$$\begin{aligned} \mathcal{D}_w(x, y) \equiv \int_0^1 ds s^2 e^{-2\hat{\mu}^2 s^2} \left[ \sqrt{x} J_{\nu+1}(s\sqrt{x}) \left( \frac{\nu}{\sqrt{y}} J_\nu(s\sqrt{y}) - s J_{\nu+1}(s\sqrt{y}) \right) \right. \\ \left. + J_\nu(s\sqrt{x}) \left( \nu J_{\nu+1}(s\sqrt{y}) - s\sqrt{y} J_\nu(s\sqrt{y}) \right) \right]. \end{aligned} \quad (3.22)$$

Looking at eq. (2.14) and noting that  $\mathcal{D}_w$  is the derivative of  $\mathcal{K}_w$  with respect to the second argument, eq. (3.22) with  $x = y$  also provides the mass-degenerate two-flavour partition function,

$$Z_w^{(N_f=2, \nu)}(\hat{\mu}; \hat{m}, \hat{m}) \sim \int_0^1 ds s^3 e^{-2\hat{\mu}^2 s^2} \hat{m} \left( J_{\nu+1}(s\hat{m}) J_{\nu-1}(s\hat{m}) - J_\nu(s\hat{m})^2 \right), \quad (3.23)$$

after using an identity for Bessel functions. The two-flavour density of the real and imaginary eigenvalues can readily be obtained from the above building blocks, using eqs. (3.8) and (3.9),

$$\rho_w^{(N_f=2, (i)\mathbb{R})}(\xi; \hat{m}_1, \hat{m}_2) = \rho_w^{(0, (i)\mathbb{R})}(\xi) + 2|\xi| \frac{\mathcal{K}_w(\xi^2, \hat{m}_2^2) G_w(\hat{m}_1^2, \xi^2) - \mathcal{K}_w(\xi^2, \hat{m}_1^2) G_w(\hat{m}_2^2, \xi^2)}{\mathcal{K}_w(\hat{m}_1^2, \hat{m}_2^2)} \quad (3.24)$$

with  $G_w$  defined in eq. (3.16). However, there is no simple expression for the degenerate-mass limit in this case.

Our second unquenched example is the case of a single flavour ( $N_f = 1$ ). The density of complex eigenvalues reads

$$\rho_w^{(N_f=1, \mathbb{C})}(\xi; \hat{m}) = \rho_w^{(0, \mathbb{C})}(\xi) + 4|\xi|^2 \hat{g}_w(\xi^{*2}, \xi^2) \frac{q_w(\xi^2) \mathcal{K}_w(\xi^{*2}, \hat{m}^2) - q_w(\xi^{*2}) \mathcal{K}_w(\xi^2, \hat{m}^2)}{q_w(\hat{m}^2)}, \quad (3.25)$$

which includes the second building block eq. (2.9),

$$q_w(z) = 2^{-\nu} e^{-\hat{\mu}^2/2} J_\nu(\sqrt{z}).$$

For the density of real and imaginary eigenvalues we again encounter the problem of non-commutativity of the large- $N$  limit and integration. By handling this issue similarly to the quenched case (see above), we obtain

$$\rho_w^{(N_f=1, (i)\mathbb{R})}(\xi; \hat{m}) = \rho_w^{(N_f=0, (i)\mathbb{R})}(\xi) + 2|\xi| \frac{q_w(\xi^2) G_w(\hat{m}^2, \xi^2) - Q_w(\xi^2) \mathcal{K}_w(\xi^2, \hat{m}^2)}{q_w(\hat{m}^2)}, \quad (3.26)$$

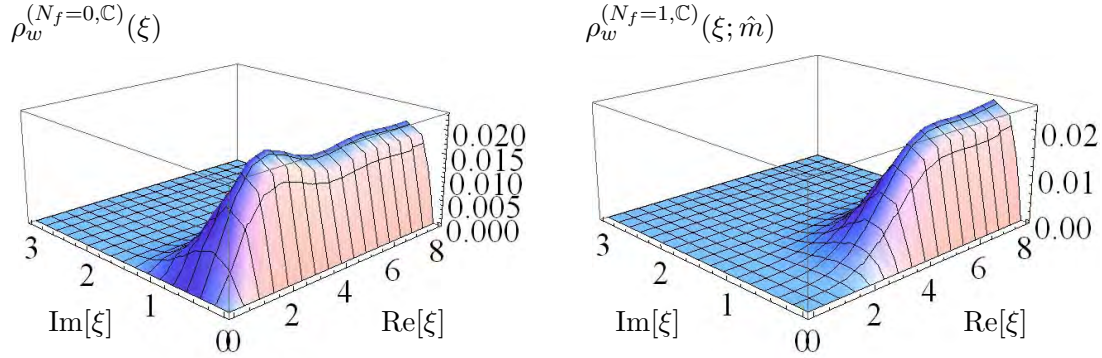


**Figure 3.** Quenched (left) and  $N_f = 1$  (right) spectral density of complex Dirac eigenvalues at weak non-Hermiticity, both for  $\hat{\mu} = \sqrt{0.2}$  at  $\nu = 0$ . The right figure is in the chiral limit ( $\hat{m} = 0$ ).

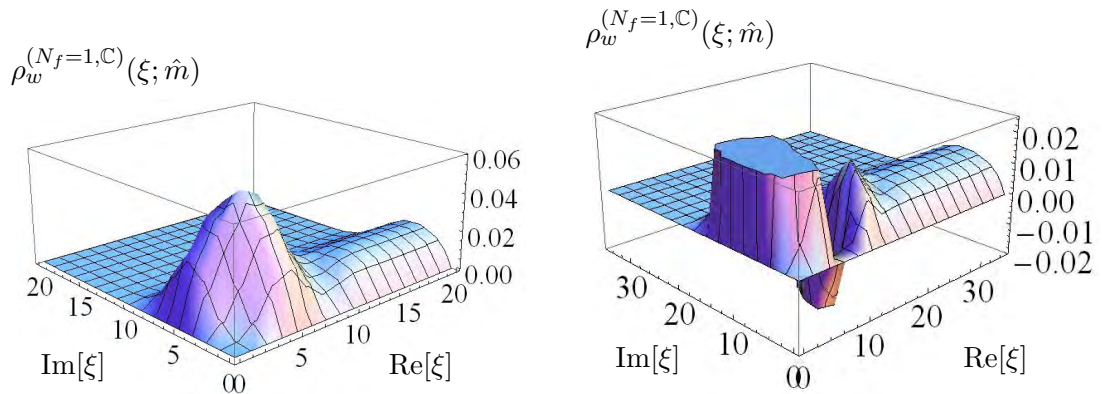


**Figure 4.** The  $N_f = 1$  spectral density of complex Dirac eigenvalues at weak non-Hermiticity for  $\hat{\mu} = 1.8$  (left) and  $\hat{\mu} = 2.5$  (right) at  $\nu = 0$  in the chiral limit ( $\hat{m} = 0$ ). Here and in the following the peaks of the oscillations are clipped.

where

$$Q_w(x) \equiv \frac{\hat{h}_w(x)}{[\text{sgn}(x)]^{\nu/2}} \left\{ \left( (-i)^\nu \int_{-\infty}^0 dy + \frac{2}{[\text{sgn}(x)]^{\nu/2}} \int_0^x dy \right) q_w(y) \hat{h}_w(y) - 2^{3-\nu} \sqrt{\pi} e^{\hat{\mu}^2/2} \left( \frac{\hat{\mu}^{\nu+2} E_{\frac{1-\nu}{2}}(\hat{\mu}^2)}{\Gamma(\frac{\nu+1}{2})} + \hat{\mu} \right) \right\}. \quad (3.27)$$

The proof follows along similar lines to that of  $G_w(u, v)$ .

In figures 3–5 we show plots of  $\rho_w^{(N_f=0,C)}(\xi)$  from eq. (3.13) and  $\rho_w^{(N_f=1,C)}(\xi; \hat{m})$  from eq. (3.25) for several values of  $\hat{\mu}$  and  $\hat{m}$ . (Due to the symmetry  $\rho_w^{(N_f,C)}(\xi) = \rho_w^{(N_f,C)}(\xi^*) = \rho_w^{(N_f,C)}(-\xi)$  we only present the result in the first quadrant. The quark masses are taken to be imaginary as our Dirac operator is symmetric at  $\mu = 0$ .) For small  $\hat{\mu}$  (figure 3), the effect of the massless flavour is to deplete the spectral density near the origin. As  $\hat{\mu}$  increases (figures 4 and 5), qualitatively different effects emerge. In the region between the location of the mass (in this case, the origin) and the edge of the spectrum, there appears a domain of strong oscillations with the shape of an ellipse that grows in its peak size and

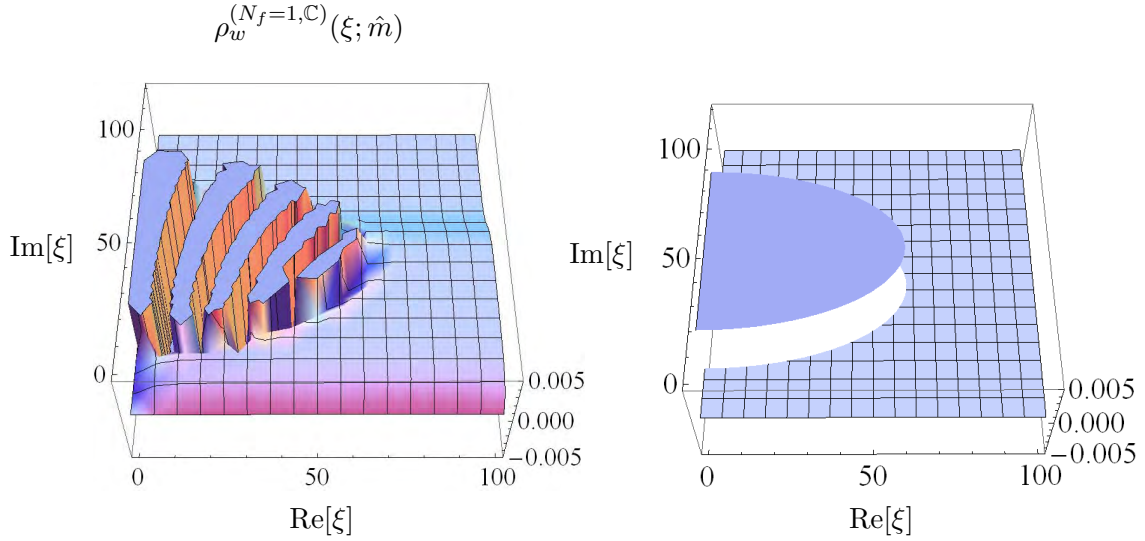


**Figure 5.** Left:  $N_f = 1$  spectral density of complex Dirac eigenvalues at weak non-Hermiticity for  $\hat{\mu} = 6$  and  $\hat{m} = 20i$  at  $\nu = 0$ . Right: Envelope of the oscillating region given by eq. (4.14), see section 4.1 for more details.

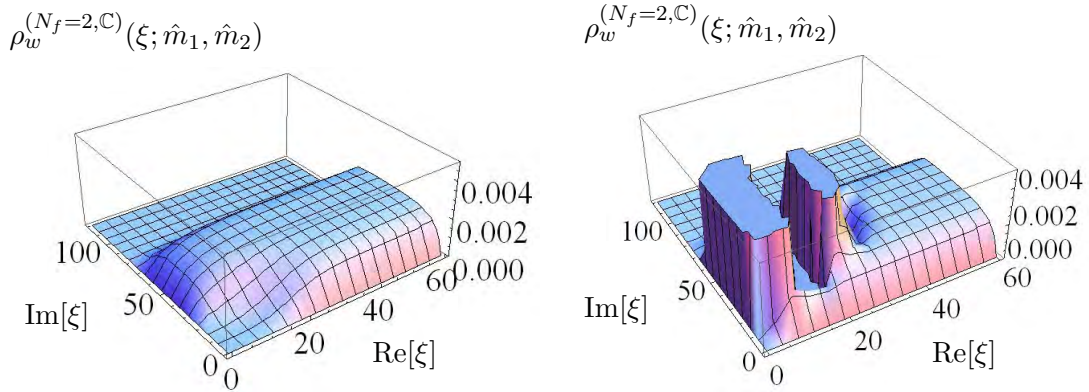


**Figure 6.** The  $N_f = 2$  spectral density of complex Dirac eigenvalues at weak non-Hermiticity for  $\hat{\mu} = 6$  and  $\nu = 0$ , for  $\hat{m}_1 = \hat{m}_2 = 10i$  (left) and  $\hat{m}_1 = 10i$  and  $\hat{m}_2 = 70i$  (right). In the right figure only the positive part of  $\rho_w^{(N_f=2, \mathbb{C})}$  is shown for better readability.

in the number of ripples as  $\hat{\mu}$  gets larger (see section 4.1 for a detailed analysis of these oscillations).

This change in the spectrum signals the emergence of a severe sign problem. For  $N_f = 1$  the Dirac determinant is real but not necessarily positive, hence the spectral “density” could take negative values. The structure of the oscillating domain, to be analysed in more detail in section 4.1, is quite similar to the corresponding one in the non-Hermitian RMT for three-colour QCD with  $\mu \neq 0$  [27], despite the difference in symmetries between two and three colours.

Another important remark is in order. When  $\hat{m}$  becomes so large that it is located outside the support of the quenched spectrum, the spectrum shows no change as compared to the quenched case. This is consistent with the physical expectation that a heavy flavour

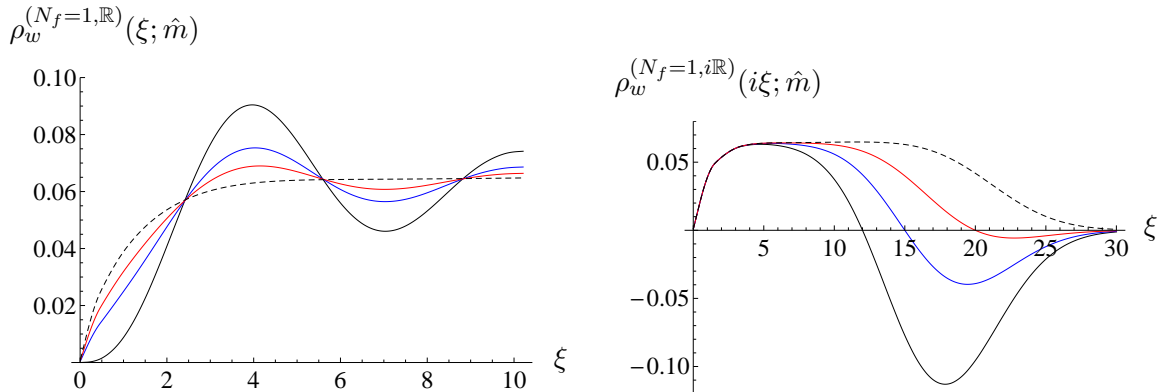


**Figure 7.** The  $N_f = 1$  spectral density of real (left) and imaginary (right) Dirac eigenvalues at weak non-Hermiticity for  $\hat{\mu} = 3$  and  $\nu = 0$ . Left:  $\hat{m} = 0.1i$  (black),  $\hat{m} = 2i$  (blue),  $\hat{m} = 3i$  (red), and quenched case (dashed). Right:  $\hat{m} = 12i$  (black),  $\hat{m} = 15i$  (blue),  $\hat{m} = 20i$  (red), and quenched case (dashed). Note that the zeros coincide with the mass values.

should effectively decouple from the rest of the system. More importantly, it suggests that the sign problem will be milder when the quark mass is larger than a certain critical value, set by the width of the quenched support. An essentially identical conclusion was reached for the three-colour RMT (see, e.g., [44] for a review), again despite the difference from our two-colour model.

Next, we turn to the plot of  $\rho_w^{(N_f=2, \mathbb{C})}(\xi; \hat{m}_1, \hat{m}_2)$  from eq. (3.20) for two sets of masses in figure 6. For degenerate masses (left), there is no sign problem and no change in the spectrum except for a depletion of eigenvalues near the location of the masses. This situation is qualitatively very similar to the symmetry class for adjoint QCD (which has no real or imaginary eigenvalues), see the figures in [28]. For widely different masses, the density develops a domain of oscillations, which resembles the  $N_f = 1$  case. This implies the decoupling of one flavour to become heavy. In section 3.3 it will be shown that a similar oscillating spectrum emerges at high density for well-separated masses for  $N_f = 2$ . This was to be anticipated from the connection between the weak and strong large- $N$  limits (see the comment in the paragraph following eq. (2.6)).

In figure 7 we show plots of  $\rho_w^{(N_f=1, (i)\mathbb{R})}(\xi; \hat{m})$  from eq. (3.26). The effect of a dynamical flavour is always stronger for the imaginary eigenvalues than for the real eigenvalues. The reason is that the partition function and densities vanish when the imaginary eigenvalues equal the (in our case) imaginary masses, see eqs. (3.4) and (3.3). Thus the imaginary density crosses the horizontal axis at the value of the mass.<sup>7</sup> Interestingly the dynamical flavour brings about an oscillatory behaviour in the real density. For both real and imaginary densities, one can clearly observe a convergence to the quenched density as the mass is increased, which leads to an effective quenching (see appendix B for an analytic confirmation of this fact).

<sup>7</sup>Using eq. (C.7) in the appendix and the positivity of the partition function for imaginary masses, one can prove for general  $N_f$  that the imaginary density cannot cross the horizontal axis at values away from the masses. This explains why a rapid oscillation as in figure 5 does not occur in the imaginary density.

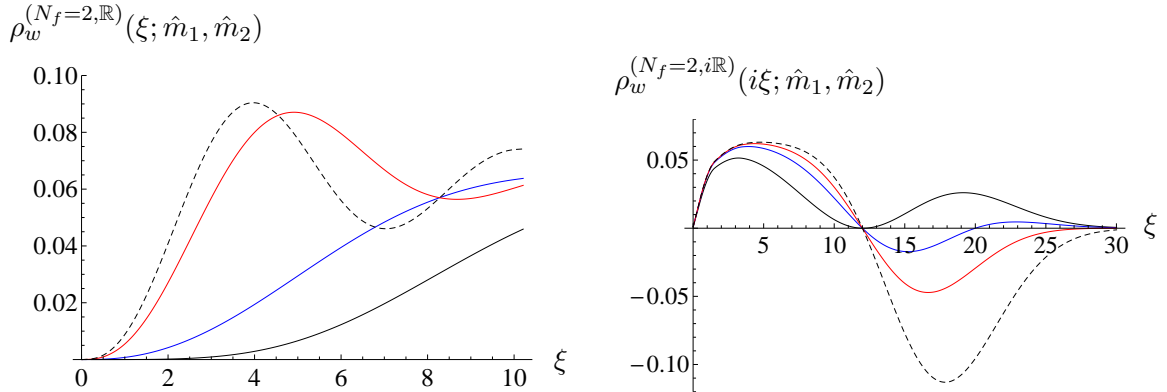


**Figure 8.** The  $N_f = 2$  spectral density of real (left) and imaginary (right) Dirac eigenvalues at weak non-Hermiticity for  $\hat{\mu} = 3$  and  $\nu = 0$ . Left:  $(\hat{m}_1, \hat{m}_2) = (0.1i, 0.1i)$  (black),  $(0.1i, 10i)$  (blue),  $(0.1i, 30i)$  (red), and  $N_f = 1$  case with  $\hat{m} = 0.1i$  (dashed). Right:  $(\hat{m}_1, \hat{m}_2) = (12i, 12i)$  (black),  $(12i, 20i)$  (blue),  $(12i, 30i)$  (red), and  $N_f = 1$  case with  $\hat{m} = 12i$  (dashed). Note that the zeros coincide with the mass values.

In figure 8 we show plots of  $\rho_w^{(N_f=2, (i)\mathbb{R})}(\xi; \hat{m}_1, \hat{m}_2)$  from eq. (3.24). We illustrate the effect of dynamical flavours by changing one of the masses while keeping the other one fixed. For both real and imaginary densities, one can clearly observe a convergence to the  $N_f = 1$  density as one of the masses is increased. Note also that the spectral density for degenerate masses is positive, as it should be, because there is no sign problem there.

Because of the issue of non-interchangeability of integration and large- $N$  limit in the weak limit, as well as in order to better understand explicitly the relation between theories with different flavour content, we have checked in appendix B that sending a subset of masses to infinity leads to the decoupling of these.

### 3.3 Eigenvalue densities at high density

In this subsection we will give the results for the spectral density in the large- $N$  limit at strong non-Hermiticity, which corresponds physically to the high-density regime. In this large- $N$  limit the rescaling of the parameters is different from the one in eq. (3.11) and is given by (see also eq. (2.6))

$$\begin{aligned} \hat{m}_f &\equiv m_f, \\ \xi &\equiv \Lambda, \end{aligned} \tag{3.28}$$

i.e., the masses and the Dirac eigenvalues, as well as  $\mu$ , need no rescaling at all. For the microscopic densities of Wishart eigenvalues we have

$$\begin{aligned} R_s^{(N_f, \mathbb{C})}(z) &\equiv \lim_{N \rightarrow \infty} R_1^{(N_f, \mathbb{C})}(z), \\ R_s^{(N_f, (i)\mathbb{R})}(x) &\equiv \lim_{N \rightarrow \infty} R_1^{(N_f, \mathbb{R})}(x), \end{aligned} \tag{3.29}$$

and the densities of Dirac eigenvalues are again obtained using the mappings in eq. (3.10). We again begin by quoting the quenched densities from [34], which will constitute the

building blocks for the new unquenched results. We have

$$\rho_s^{(N_f=0, \mathbb{C})}(\xi) = 4|\xi|^2 \hat{g}_s(\xi^{*2}, \xi^2) \mathcal{K}_s(\xi^2, \xi^{*2}), \quad (3.30)$$

where the complex weight in the strong limit is defined as

$$\begin{aligned} \hat{g}_s(z, z^*) &= -\hat{g}_s(z^*, z) \equiv 2i \operatorname{sgn}(\operatorname{Im} z) \frac{1}{|z|^\nu} g(z^*, z) \\ &= 4i \operatorname{sgn}(\operatorname{Im} z) e^{2\eta_- \operatorname{Re} z} \int_0^\infty \frac{dt}{t} e^{-\eta_+^2 t(z^2 + z^{*2}) - \frac{1}{4t} K_{\frac{\nu}{2}}(2\eta_+^2 t|z|^2)} \operatorname{erfc}(2\eta_+ \sqrt{t} |\operatorname{Im} z|) \end{aligned} \quad (3.31)$$

with  $g$  from eq. (3.6). It can be seen from that equation that the cases of general  $\mu \leq 1$  and of maximal non-Hermiticity with  $\mu = 1$  (and  $\eta_+ = \frac{1}{2}$ ) are related simply by a rescaling of the complex eigenvalue  $\eta_+ \xi^2 \rightarrow \xi^2/2$ . The same is true for the densities of the real and imaginary eigenvalues,

$$\begin{aligned} \rho_s^{(N_f=0, (i)\mathbb{R})}(\xi) &= 2|\xi| \frac{\eta_+^3}{8\pi} 2K_{\frac{\nu}{2}}(\eta_+ |\xi|^2) \left( \int_0^\infty dx' |\xi^2 - x'| 2K_{\frac{\nu}{2}}(\eta_+ |x'|) I_\nu(2\eta_+ \xi \sqrt{x'}) \right. \\ &\quad \left. + \int_{-\infty}^0 dx' |\xi^2 - x'| 2K_{\frac{\nu}{2}}(\eta_+ |x'|) J_\nu(2\eta_+ \xi \sqrt{|x'|}) \right). \end{aligned} \quad (3.32)$$

Unlike in the weak limit, in the strong limit no complications arise from an interchange of the large- $N$  limit and the integration.

The example of two non-degenerate flavours is now straightforward, and we only quote the result which includes eq. (3.30) as the first term,

$$\begin{aligned} \rho_s^{(N_f=2, \mathbb{C})}(\xi; \hat{m}_1, \hat{m}_2) \\ = \rho_s^{(0, \mathbb{C})}(\xi) + 4|\xi|^2 \hat{g}_s(\xi^{*2}, \xi^2) \frac{\mathcal{K}_s(\xi^2, \hat{m}_2^2) \mathcal{K}_s(\xi^{*2}, \hat{m}_1^2) - \mathcal{K}_s(\xi^2, \hat{m}_1^2) \mathcal{K}_s(\xi^{*2}, \hat{m}_2^2)}{\mathcal{K}_s(\hat{m}_1^2, \hat{m}_2^2)}. \end{aligned} \quad (3.33)$$

It is identical to the form of the weak result in eq. (3.20) apart from the kernel in the strong limit from eq. (2.10),

$$\mathcal{K}_s(u, v) = \frac{\eta_+^3}{8\pi} (u - v) e^{-\eta_-(u+v)} I_\nu(2\eta_+ \sqrt{uv}).$$

It is easy to obtain the limiting result for two degenerate masses which we also give here for completeness,

$$\begin{aligned} \rho_s^{(N_f=2, \mathbb{C})}(\xi; \hat{m}_1, \hat{m}_2) \\ = \rho_s^{(N_f=0, \mathbb{C})}(\xi) + 4|\xi|^2 \hat{g}_s(\xi^{*2}, \xi^2) \frac{\eta_+^3 e^{-\eta_-(\xi^2 + \xi^{*2})}}{8\pi I_\nu(2\eta_+ \hat{m}_1^2)} \left[ (\xi^2 - \xi^{*2}) |I_\nu(2\eta_+ \hat{m}_1 \xi)|^2 \right. \\ \left. + (\xi^2 - \hat{m}_1^2)(\xi^{*2} - \hat{m}_1^2) \frac{\eta_+}{\hat{m}_1} \left( I_\nu(2\eta_+ \hat{m}_1 \xi^*) \xi I_{\nu+1}(2\eta_+ \hat{m}_1 \xi) - (\xi \leftrightarrow \xi^*) \right) \right]. \end{aligned} \quad (3.34)$$

Similarly, the extension of eq. (3.32) to  $N_f = 2$  reads

$$\begin{aligned} \rho_s^{(N_f=2, (i)\mathbb{R})}(\xi; \hat{m}_1, \hat{m}_2) &= \rho_s^{(N_f=0, (i)\mathbb{R})}(\xi) + 2|\xi| \hat{h}_s(\xi^2) \int_{\mathbb{R}} dx \hat{h}_s(x) \operatorname{sgn}(\xi^2 - x) \\ &\quad \times \frac{\mathcal{K}_s(\xi^2, \hat{m}_2^2) \mathcal{K}_s(x, \hat{m}_1^2) - \mathcal{K}_s(\xi^2, \hat{m}_1^2) \mathcal{K}_s(x, \hat{m}_2^2)}{\mathcal{K}_s(\hat{m}_1^2, \hat{m}_2^2)}, \end{aligned} \quad (3.35)$$

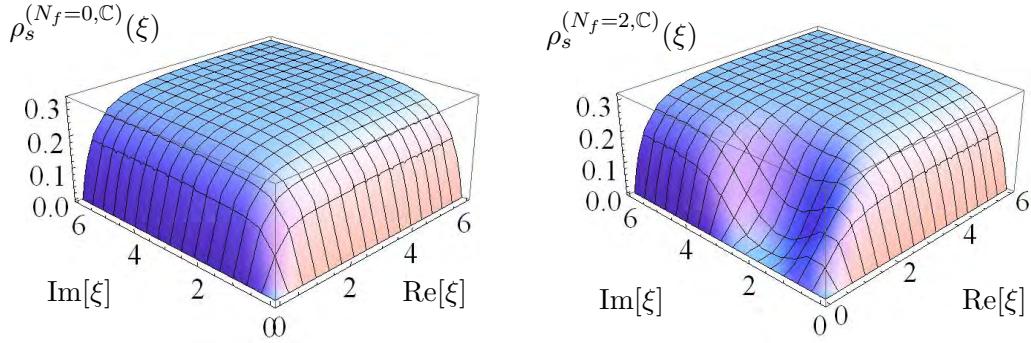


**Figure 9.** Quenched (left) and  $N_f = 2$  (right) spectral density of complex Dirac eigenvalues at maximal non-Hermiticity ( $\mu = 1$ ) for  $\nu = 0$ , with equal  $\hat{m}_1 = \hat{m}_2 = 2i$  in the right figure. Note again the similarity with adjoint QCD [28].

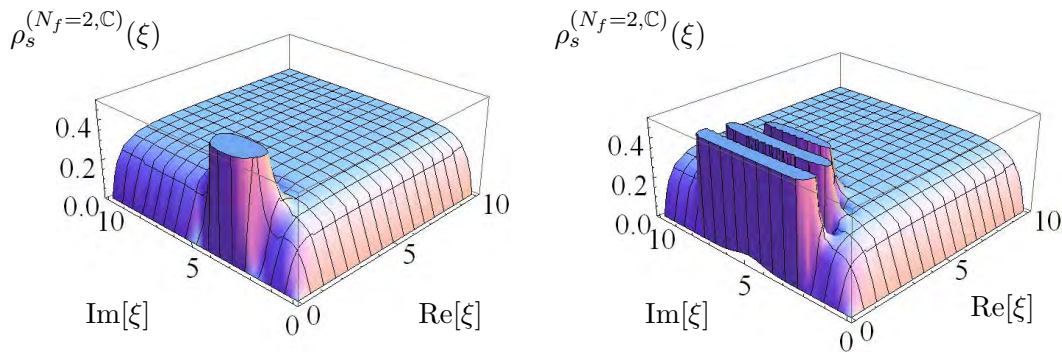


**Figure 10.** The  $N_f = 2$  spectral density of complex Dirac eigenvalues at maximal non-Hermiticity ( $\mu = 1$ ) for  $\nu = 0$  with  $(\hat{m}_1, \hat{m}_2) = (2i, 5i)$  (left) and  $(\hat{m}_1, \hat{m}_2) = (2i, 8i)$  (right). In the right figure the negative part of  $\rho_s$  is cut for better readability.

where the strong limit of the real weight is defined as

$$\hat{h}_s(z) \equiv \frac{1}{(-z)^{\nu/2}} h(z) = 2 \frac{|z|^{\nu/2}}{(-z)^{\nu/2}} e^{\eta-z} K_{\frac{\nu}{2}}(\eta+|z|). \quad (3.36)$$

The density  $\rho_s^{(N_f=2,\mathbb{C})}(\xi; \hat{m}_1, \hat{m}_2)$  is plotted in figures 9 and 10. In the former the quenched result is also included for comparison. (Again, we only present the result in the first quadrant because of the symmetry  $\rho_s^{(N_f,\mathbb{C})}(\xi) = \rho_s^{(N_f,\mathbb{C})}(\xi^*) = \rho_s^{(N_f,\mathbb{C})}(-\xi)$ , and we take the quark masses to be imaginary as our Dirac operator is symmetric at  $\mu = 0$ . Since the difference between  $0 < \mu < 1$  and  $\mu = 1$  is trivial we set  $\mu = 1$  in the figures.) We observe that the effect of dynamical flavours with equal masses is to simply generate a dip in the quenched spectrum. The effect of unequal masses is qualitatively different. For a sufficiently large mass difference, the spectrum exhibits a domain of strong oscillations, taking both positive and negative values, which signals the appearance of the sign problem. We caution that sending one of the masses to infinity does not yield  $\rho_s^{(N_f=1,\mathbb{C})}(\xi; \hat{m})$  but merely makes the oscillating domain extend to the entire spectrum.<sup>8</sup>

<sup>8</sup>This is not in contradiction with the usual decoupling of heavy flavours, see appendix B, since in the

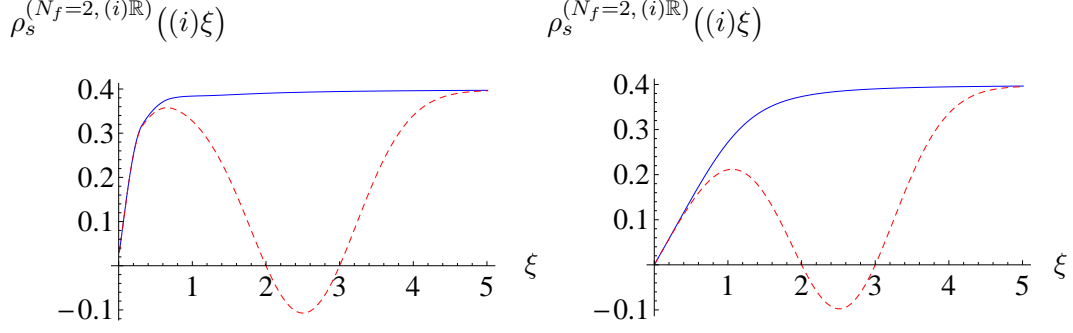


**Figure 11.** The  $N_f = 2$  spectral density of Dirac eigenvalues at maximum non-Hermiticity ( $\mu = 1$ ) for  $(\hat{m}_1, \hat{m}_2) = (2i, 3i)$  at  $\nu = 0$  (left) and  $\nu = 2$  (right). The densities of both real (blue full line) and imaginary (red dashed line) eigenvalues are displayed in the same plot for comparison. The latter again has zeros at the locations of the masses.

The density  $\rho_s^{(N_f=2, (i)\mathbb{R})}((i)\xi; \hat{m}_1, \hat{m}_2)$  is plotted in figure 11. As in the case of weak non-Hermiticity, the density of imaginary eigenvalues goes through zero at  $\xi = i\hat{m}_1$  and  $\xi = i\hat{m}_2$ . However, unlike in the case of weak non-Hermiticity, no oscillation of the density of real eigenvalues is observed. A more detailed analysis of the sign problem will be presented in section 4.

We now consider the case of four quark flavours, which is interesting since at high density  $N_f = 2$  and  $N_f \geq 4$  (even) have distinct chiral symmetry breaking patterns and a new class of Nambu-Goldstone bosons emerges for  $N_f \geq 4$  [13]. With non-degenerate masses, we have to expand the Pfaffian of a  $6 \times 6$  matrix in order to write down the complex density explicitly. The result is

$$\begin{aligned}
\rho_s^{(N_f=4, \mathbb{C})}(\xi; \{\hat{m}\}_4) &= \rho_s^{(N_f=0, \mathbb{C})}(\xi) \\
&+ \frac{4|\xi|^2 \hat{g}_s(\xi^{*2}, \xi^2)}{\mathcal{K}_s(\hat{m}_1^2, \hat{m}_2^2) \mathcal{K}_s(\hat{m}_3^2, \hat{m}_4^2) - \mathcal{K}_s(\hat{m}_1^2, \hat{m}_3^2) \mathcal{K}_s(\hat{m}_2^2, \hat{m}_4^2) + \mathcal{K}_s(\hat{m}_1^2, \hat{m}_4^2) \mathcal{K}_s(\hat{m}_2^2, \hat{m}_3^2)} \\
&\times \left\{ \mathcal{K}_s(\hat{m}_1^2, \xi^{*2}) \mathcal{K}_s(\hat{m}_2^2, \xi^2) \mathcal{K}_s(\hat{m}_3^2, \hat{m}_4^2) - \mathcal{K}_s(\hat{m}_1^2, \xi^2) \mathcal{K}_s(\hat{m}_2^2, \xi^{*2}) \mathcal{K}_s(\hat{m}_3^2, \hat{m}_4^2) \right. \\
&- \mathcal{K}_s(\hat{m}_1^2, \xi^{*2}) \mathcal{K}_s(\hat{m}_2^2, \hat{m}_4^2) \mathcal{K}_s(\hat{m}_3^2, \xi^2) + \mathcal{K}_s(\hat{m}_1^2, \hat{m}_4^2) \mathcal{K}_s(\hat{m}_2^2, \xi^{*2}) \mathcal{K}_s(\hat{m}_3^2, \xi^2) \\
&+ \mathcal{K}_s(\hat{m}_1^2, \xi^2) \mathcal{K}_s(\hat{m}_2^2, \hat{m}_4^2) \mathcal{K}_s(\hat{m}_3^2, \xi^{*2}) - \mathcal{K}_s(\hat{m}_1^2, \hat{m}_4^2) \mathcal{K}_s(\hat{m}_2^2, \xi^2) \mathcal{K}_s(\hat{m}_3^2, \xi^{*2}) \\
&+ \mathcal{K}_s(\hat{m}_1^2, \xi^{*2}) \mathcal{K}_s(\hat{m}_2^2, \hat{m}_3^2) \mathcal{K}_s(\hat{m}_4^2, \xi^2) - \mathcal{K}_s(\hat{m}_1^2, \hat{m}_3^2) \mathcal{K}_s(\hat{m}_2^2, \xi^{*2}) \mathcal{K}_s(\hat{m}_4^2, \xi^2) \\
&+ \mathcal{K}_s(\hat{m}_1^2, \hat{m}_2^2) \mathcal{K}_s(\hat{m}_3^2, \xi^{*2}) \mathcal{K}_s(\hat{m}_4^2, \xi^2) - \mathcal{K}_s(\hat{m}_1^2, \xi^2) \mathcal{K}_s(\hat{m}_2^2, \hat{m}_3^2) \mathcal{K}_s(\hat{m}_4^2, \xi^{*2}) \\
&\left. + \mathcal{K}_s(\hat{m}_1^2, \hat{m}_3^2) \mathcal{K}_s(\hat{m}_2^2, \xi^2) \mathcal{K}_s(\hat{m}_4^2, \xi^{*2}) - \mathcal{K}_s(\hat{m}_1^2, \hat{m}_2^2) \mathcal{K}_s(\hat{m}_3^2, \xi^2) \mathcal{K}_s(\hat{m}_4^2, \xi^{*2}) \right\}.
\end{aligned} \tag{3.37}$$

Plots of  $\rho_s^{(N_f=4, \mathbb{C})}(\xi; \{\hat{m}\}_4)$  are shown in figures 12 and 13. It is seen that  $N_f = 4$  flavours roughly amount to two pairs of  $N_f = 2$  flavours, each of which shows either a dip or a domain of strong oscillations.

---

strong limit we are restricted to even  $N_f$ .

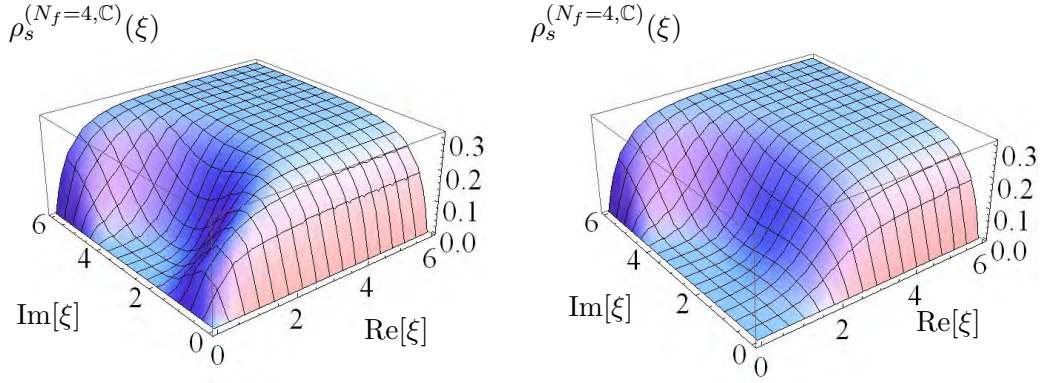


**Figure 12.** The  $N_f = 4$  spectral density of complex Dirac eigenvalues at maximal non-Hermiticity ( $\mu = 1$ ) for  $\hat{m}_1 = \hat{m}_2 = \hat{m}_3 = \hat{m}_4 = 3i$  at  $\nu = 0$  (left) and  $\nu = 6$  (right).

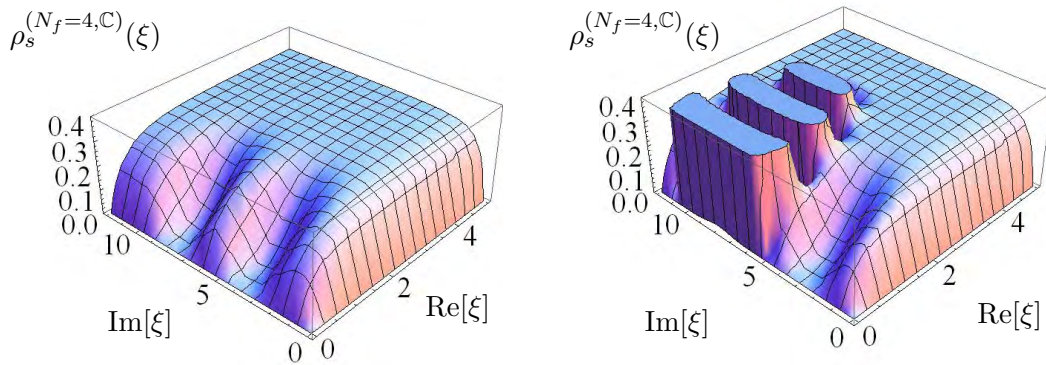


**Figure 13.** Same as figure 12 but for  $\hat{m}_1 = \hat{m}_2 = 4i$ ,  $\hat{m}_3 = \hat{m}_4 = 8i$  (left) and  $\hat{m}_1 = \hat{m}_2 = 3i$ ,  $\hat{m}_3 = 5i$ ,  $\hat{m}_4 = 11i$  (right), both at  $\nu = 0$ . Note that the scales for  $\text{Re}[\xi]$  and  $\text{Im}[\xi]$  are different. In the right figure the negative part of  $\rho_s$  is cut for better readability.

## 4 The sign problem

### 4.1 Analysis of oscillations of the Dirac spectrum

If we choose non-identical masses the spectral densities show interesting behaviour. In this section, we will consider in particular the case of  $N_f = 2$  with  $\hat{m}_1 \neq \hat{m}_2$ , and the case of  $N_f = 1$  in the weak non-Hermiticity limit. As can be seen from a direct inspection of the expression (2.1) for the partition function, the presence of non-degenerate masses can lead to “probabilities” which, although still real-valued, may be negative in certain regions. This is perhaps not unexpected. However, what may be surprising is that there are regions of the complex plane in which the eigenvalue density function seems to oscillate from positive to negative values quite dramatically. We present here a straightforward explanation.

For simplicity, we first consider the strong limit which was discussed in section 3.3. In the quenched case, the complex Dirac eigenvalue density is essentially constant everywhere apart from close to the real and imaginary axes, where it vanishes. As we discussed earlier in eq. (3.19), the unquenched density can be written as a correction to the quenched case.

From eq. (3.33), the correction in this case is

$$\Delta\rho_s^{(N_f=2,\mathbb{C})}(\xi; \hat{m}_1, \hat{m}_2) = \frac{4|\xi|^2 \hat{g}_s(\xi^{*2}, \xi^2)}{\mathcal{K}_s(\hat{m}_1^2, \hat{m}_2^2)} (-2i) \operatorname{Im} \left\{ \mathcal{K}_s(\xi^2, \hat{m}_1^2) \mathcal{K}_s(\xi^{*2}, \hat{m}_2^2) \right\}, \quad (4.1)$$

where the weight function  $\hat{g}_s(z^*, z)$  was given in eq. (3.31). We next insert the explicit form of the strong kernel from eq. (2.10), and, after noting that a number of factors cancel, we get

$$\begin{aligned} \Delta\rho_s^{(N_f=2,\mathbb{C})}(\xi; \hat{m}_1, \hat{m}_2) &= 4|\xi|^2 \left[ \frac{\eta_+^3}{8\pi} \right] \hat{g}_s(\xi^{*2}, \xi^2) \frac{\exp[-\eta_-(\xi^2 + \xi^{*2})]}{(\hat{m}_1^2 - \hat{m}_2^2) I_\nu(2\eta_+ \hat{m}_1 \hat{m}_2)} \\ &\times (-2i) \operatorname{Im} \left\{ (\xi^2 - \hat{m}_1^2)(\xi^{*2} - \hat{m}_2^2) I_\nu(2\eta_+ \xi \hat{m}_1) I_\nu(2\eta_+ \xi^* \hat{m}_2) \right\}. \end{aligned} \quad (4.2)$$

Here,  $\eta_+$  and  $\eta_-$  are as defined in eq. (2.11). So far everything is exact. However, we now make two approximations. First, we approximate  $\hat{g}_s(\xi^{*2}, \xi^2)$  by using the following argument. For the quenched case, away from the axes, the Dirac density is essentially flat, i.e., it is equal to some constant which we could determine exactly, but here we shall simply denote it by  $\rho_S$ . Therefore, from eq. (3.30), we have

$$4|\xi|^2 \hat{g}_s(\xi^{*2}, \xi^2) \mathcal{K}_s(\xi^{*2}, \xi^2) \approx \rho_S. \quad (4.3)$$

On inserting the explicit form of the strong kernel, and rearranging, we have

$$4|\xi|^2 \left[ \frac{\eta_+^3}{8\pi} \right] \hat{g}_s(\xi^{*2}, \xi^2) \exp[-\eta_-(\xi^2 + \xi^{*2})] \approx \frac{\rho_S}{(\xi^2 - \xi^{*2}) I_\nu(2\eta_+ |\xi|^2)}, \quad (4.4)$$

and so, away from the axes,

$$\Delta\rho_s^{(N_f=2,\mathbb{C})}(\xi; \hat{m}_1, \hat{m}_2) \approx \frac{(-2i) \rho_S \operatorname{Im} \left\{ (\xi^2 - \hat{m}_1^2)(\xi^{*2} - \hat{m}_2^2) I_\nu(2\eta_+ \xi \hat{m}_1) I_\nu(2\eta_+ \xi^* \hat{m}_2) \right\}}{(\hat{m}_1^2 - \hat{m}_2^2) I_\nu(2\eta_+ \hat{m}_1 \hat{m}_2) (\xi^2 - \xi^{*2}) I_\nu(2\eta_+ |\xi|^2)}. \quad (4.5)$$

Our second approximation is to replace each modified Bessel function with its large-argument asymptotic limit, namely

$$I_\nu(z) \sim \frac{e^z}{\sqrt{2\pi z}} \quad (4.6)$$

for  $-\frac{\pi}{2} < \arg(z) < \frac{\pi}{2}$ , i.e., in the right half-plane. After simplification, this gives (in the right half-plane, and sufficiently far away from the origin and from the axes)

$$\begin{aligned} \Delta\rho_s^{(N_f=2,\mathbb{C})}(\xi; \hat{m}_1, \hat{m}_2) &\approx \frac{(-2i) \rho_S e^{-2\eta_+(\hat{m}_1 \hat{m}_2 + |\xi|^2)}}{(\hat{m}_1^2 - \hat{m}_2^2)(\xi^2 - \xi^{*2})} \operatorname{Im} \left\{ (\xi^2 - \hat{m}_1^2)(\xi^{*2} - \hat{m}_2^2) e^{2\eta_+(\xi \hat{m}_1 + \xi^* \hat{m}_2)} \right\} \\ &= \frac{(-2i) \rho_S}{(\hat{m}_1^2 - \hat{m}_2^2)(\xi^2 - \xi^{*2})} \exp \left[ 2\eta_+((\hat{m}_1 + \hat{m}_2)x - |\xi|^2 - \hat{m}_1 \hat{m}_2) \right] \\ &\times \operatorname{Im} \left\{ (\xi^2 - \hat{m}_1^2)(\xi^{*2} - \hat{m}_2^2) \left( \cos(2\eta_+(\hat{m}_1 - \hat{m}_2)\hat{y}) + i \sin(2\eta_+(\hat{m}_1 - \hat{m}_2)\hat{y}) \right) \right\}, \end{aligned} \quad (4.7)$$

where we have written  $\hat{x} \equiv \text{Re } \xi$  and  $\hat{y} \equiv \text{Im } \xi$ . We can regard this function as being the product of an envelope (the exponential), some polynomials in  $\xi$  and  $\xi^*$ , and an oscillatory function of  $\hat{y}$ . Let us consider each in turn.

To understand the behaviour of the exponential part, we can determine the contours in the  $\xi$ -plane where this part takes constant values. We can equivalently perform this analysis on the exponent. So we look for the solution of

$$(\hat{m}_1 + \hat{m}_2)\hat{x} - |\xi|^2 - \hat{m}_1\hat{m}_2 = k, \quad (4.8)$$

where  $k$  is some constant. Writing  $|\xi|^2 = \hat{x}^2 + \hat{y}^2$ , and rearranging, we have

$$\left(\hat{x} - \frac{\hat{m}_1 + \hat{m}_2}{2}\right)^2 + \hat{y}^2 = \left(\frac{\hat{m}_1 - \hat{m}_2}{2}\right)^2 - k \equiv r^2. \quad (4.9)$$

This is, of course, the equation of a circle of radius  $r$ , centred on the point  $\xi = (\hat{m}_1 + \hat{m}_2)/2$ . The exponential function equals unity when  $k = 0$ , i.e., when the circle passes through the points  $\xi = \hat{m}_1$  and  $\xi = \hat{m}_2$ . Crudely speaking, this marks the boundary of the region where the correction is “significant” when compared with the quenched case (where the density equals  $\rho_S$ ). Points inside this circle have  $k > 0$ , so the circle marks the boundary of a peak (rather than a dip) in the complex plane. The maximal value of this peak is  $\exp(2\eta_+ k_{\text{max}})$ , where

$$k_{\text{max}} = \left(\frac{\hat{m}_1 - \hat{m}_2}{2}\right)^2, \quad (4.10)$$

so the peak grows very rapidly indeed with the difference between  $\hat{m}_1$  and  $\hat{m}_2$ . Of course, our approximations are not valid at the centre of the circle since this lies on the  $\hat{x}$ -axis, and so this argument is merely indicative of the orders of magnitude that we might expect to observe in the density itself.

The polynomials  $(\xi^2 - \hat{m}_1^2)(\xi^{*2} - \hat{m}_2^2)$  in eq. (4.7) result in a repulsion of eigenvalues from the points  $\pm\hat{m}_1$  and  $\pm\hat{m}_2$ , similar to what we observed in the case of identical masses.

Finally, if we combine the oscillatory part of eq. (4.7) with the  $(\xi^2 - \xi^{*2})^{-1}$  factor, then we get an oscillating function of  $\hat{y}$  which is symmetric (even), and which has a constant “wavelength”

$$\lambda = \frac{\pi}{\eta_+ (\hat{m}_1 - \hat{m}_2)}. \quad (4.11)$$

In other words, this constitutes a set of ridges and troughs parallel to the real axis.

Therefore, what we observe in the total density is a circular “peak” of fairly dramatic oscillations, but these are almost completely suppressed elsewhere in the complex plane. There is also some repulsion from the location of the masses, although the exponential effect causing the peak is generally more significant. The number of oscillations visible will therefore be given by

$$N_{\text{oscillations}} \approx \frac{\eta_+ (\hat{m}_1 - \hat{m}_2)^2}{\pi}, \quad (4.12)$$

and we can say that no oscillations will be seen if, roughly speaking,

$$|\hat{m}_1 - \hat{m}_2| < \sqrt{\frac{\pi}{\eta_+}}. \quad (4.13)$$

These same conclusions can also be obtained directly from the group integral eq. (2.5). On making an ansatz for the matrices  $U, V \in U(4)$  and keeping only the degrees of freedom that are expected to be relevant, a mean-field analysis reveals the same equations for the boundary and height of the oscillations.

For the weak non-Hermiticity limit, a similar analysis can be performed, although the situation here is slightly more complicated because we need to use not one, but two approximations for the kernel, depending on the average of the arguments.

When we have two masses, both located inside the strip that contains the quenched eigenvalues (and both taken to be purely imaginary), then we find that the situation is similar to the strong case above; there is a circular region of oscillations, with the boundary of the oscillating region passing through the two masses. Indeed, one can map the weak non-Hermiticity case onto the case of maximal non-Hermiticity (with  $\mu = 1$ ) by making a simple scaling of masses and eigenvalues by  $1/2\hat{\mu}$ , and then the earlier results eqs. (4.11), (4.12) and (4.13) for the strong case also hold true here.

If we have a single mass located within the strip at  $\hat{m} = i\eta$ , then we get an elliptical region of oscillations, given in fact by the same equation as for the corresponding situation in three-colour QCD [45, eq. (41)] where it was derived from an ansatz,

$$\frac{x^2}{\left(\frac{2}{\sqrt{3}}(2\hat{\mu}^2 - \eta)\right)^2} + \frac{\left(y - \frac{4\hat{\mu}^2 + \eta}{3}\right)^2}{\left(\frac{2}{3}(2\hat{\mu}^2 - \eta)\right)^2} = 1. \quad (4.14)$$

A comparison of this formula with the exact spectral density is given in figure 5. Conversely, a single mass located outside the strip has virtually no effect whatsoever on the density.

The  $N_f = 2$  case with one of the masses considerably far outside the strip (in fact, beyond a (finite) critical point for which we can solve) is both qualitatively and quantitatively very similar to the  $N_f = 1$  case; we refer to Appendix B for further details on the decoupling as one of the masses is taken progressively larger. However, there is a third distinct intermediate regime where one mass is inside the strip, and the other is outside the strip, but below the critical point. Here, we find that the region of oscillations lies part-way between a circle and an ellipse.

It would be interesting to study the effects of the oscillations analysed in this section on the chiral condensate, along the lines of [39, 40]. This is left for future work.

## 4.2 Average sign factor

### 4.2.1 Introductory remarks

In this section we study the severity of the sign problem by looking at the average sign of the Dirac determinant. The definition of such an average is not unique, and we will use the following guiding principles to define an average that behaves reasonably:

- The average should be bounded by 1 from above.
- Starting at 1 for  $\mu = 0$  (or degenerate masses) the average should be a decreasing function of  $\mu$  (or the mass difference).

Let us illustrate the problem of finding a proper definition using the case of three-colour QCD (QCD3), which has been well studied in the RMT framework [46–48]. If we denote the complex phase of  $\det[\mathcal{D} + m]$  by  $e^{i\theta}$ , the authors proposed to compute

$$\langle e^{2i\theta} \rangle_{N_f}^{\text{QCD3}} \equiv \left\langle \frac{\det[\mathcal{D}(\mu) + m]}{\det[\mathcal{D}(\mu) + m]^\dagger} \right\rangle_{N_f}^{\text{QCD3}}, \quad (4.15)$$

which gives the expectation value of twice the phase in the case that the determinant is complex. Had we chosen the opposite ratio on the right-hand side instead, this would naively have led to  $\langle e^{-2i\theta} \rangle_{N_f}$ . However, for  $N_f = 1$  we have in three-colour QCD

$$\left\langle \frac{\det[\mathcal{D} + m]^\dagger}{\det[\mathcal{D} + m]} \right\rangle_{N_f=1}^{\text{QCD3}} = \frac{\langle \det[\mathcal{D} + m]^\dagger \rangle_{N_f=0}^{\text{QCD3}}}{\langle \det[\mathcal{D} + m] \rangle_{N_f=0}^{\text{QCD3}}} = 1 \quad (4.16)$$

because the expectation value in denominator and numerator (also called characteristic polynomial) is equal and  $\mu$ -independent [49]. Obviously this would contradict the second of our criteria above. Note that in contrast using the definition (4.15) the ratio is not equal to 1, even for  $N_f = 1$ .

Our definition of the average sign for two-colour QCD, which we will use throughout this section, is

$$p^{(N_f)}(\mu; \{m\}) \equiv \left\langle \text{sgn} \prod_{f=1}^{N_f} \det[D(\mu) + m_f] \right\rangle_{\|\!|N_f\!\|}, \quad (4.17)$$

where the average is computed in a sign-quenched theory denoted by  $\|\!|N_f\!\|$  (i.e., only the absolute values of the determinants appear in the measure). We recall that in the strong limit we always need  $N_f$  to be even. In the next two subsections we will consider two particular cases, the weak limit with one flavour, where

$$p_w^{(N_f=1)}(\hat{\mu}; \hat{m}) = \lim_{N \rightarrow \infty, \text{weak}} p^{(N_f=1)}(\mu; m), \quad (4.18)$$

and the strong limit with two flavours, where

$$p_s^{(N_f=2)}(\mu; \hat{m}_1, \hat{m}_2) = \lim_{N \rightarrow \infty, \text{strong}} p^{(N_f=2)}(\mu; m_1, m_2). \quad (4.19)$$

We shall see explicitly from these two cases that our guiding principles are satisfied.

We finish this subsection by commenting on possible bad choices for the average sign. Due to the obvious inequality

$$\langle |\det[\mathcal{D} + m]| \rangle_{N_f=0} \geq \langle \det[\mathcal{D} + m] \rangle_{N_f=0} \quad (4.20)$$

we have

$$\left\langle \frac{\det[\mathcal{D} + m]}{|\det[\mathcal{D} + m]|} \right\rangle_{N_f=1} = \left\langle \frac{|\det[\mathcal{D} + m]|}{\det[\mathcal{D} + m]} \right\rangle_{N_f=1} \geq 1, \quad (4.21)$$

and hence a ratio of this kind, which would have been the natural generalisation of eq. (4.15), can be ruled out. A second choice that leads to an inconsistency is the following. Because the sign problem can be turned on by detuning the masses of two originally degenerate flavours one might consider

$$\left\langle \frac{\det[\mathcal{D}(\mu) + m_1] \det[\mathcal{D}(\mu) + m_2]}{\det[\mathcal{D}(\mu) + m_0]^2} \right\rangle_{N_f}, \quad (4.22)$$

where in the denominator we have two degenerate masses  $m_0$ . One caveat is that the choice of  $m_0$  in the denominator is ambiguous. For small  $m_1 - m_2$  one might think that any of the choices  $m_0 = m_1, m_2, (m_1 + m_2)/2, \sqrt{m_1 m_2}$  would be acceptable. However, using the latter choice we can show that in the strong limit this leads to a quantity that is always unity. Moreover, in the weak limit or for other choices of  $m_0$  the quantity in eq. (4.22) goes to zero more rapidly for larger topology. This contradicts our expectation, which was confirmed in RMT studies of three-colour QCD [50], that a larger number of exactly zero eigenvalues should push the density away from the origin (where the oscillations are strong) and thus mitigate the average sign problem.

#### 4.2.2 Average sign at low density

Let us consider the case  $N_f = 1$  in the limit of weak non-Hermiticity. Although the sign-quenched partition function does not permit a field-theoretical interpretation like QCD with nonzero isospin chemical potential, it is still possible to compute it as a mathematical entity by RMT. In appendix C.3 we derive

$$\begin{aligned} \mathcal{Z}_w^{(N_f=1, \nu)}(\hat{\mu}; \hat{m}) &\equiv \lim_{N \rightarrow \infty, \text{weak}} \langle |\det[\mathcal{D}(\mu) + m]| \rangle_{N_f=0} \\ &\sim -\hat{\mu} e^{\hat{\mu}^2/2} \frac{G_w(\hat{m}^2, \hat{m}^2)}{\hat{h}_w(\hat{m}^2)}. \end{aligned} \quad (4.23)$$

This result essentially follows from the quenched real spectral density. Combining it with eq. (2.15),

$$\mathcal{Z}_w^{(N_f=1, \nu)}(\hat{\mu}; \hat{m}) \sim q_w(\hat{m}^2),$$

we obtain the average sign factor in the weak limit,

$$p_w^{(N_f=1)}(\hat{\mu}; \hat{m}) = \frac{\mathcal{Z}_w^{(N_f=1, \nu)}(\hat{\mu}; \hat{m})}{\mathcal{Z}_w^{(N_f=1, \nu)}(\hat{\mu}; \hat{m})} \sim -\frac{\hat{h}_w(\hat{m}^2) q_w(\hat{m}^2)}{\hat{\mu} e^{\hat{\mu}^2/2} G_w(\hat{m}^2, \hat{m}^2)}. \quad (4.24)$$

The normalisation of  $p_w^{(N_f=1)}(\hat{\mu}; \hat{m})$  can be uniquely determined from the requirement  $p_w^{(N_f=1)}(0, \hat{m}) = 1$ .

In figure 14 we depict how  $p_w^{(N_f=1)}(\hat{\mu}; \hat{m})$  depends on  $\hat{\mu}$  for several values of  $\hat{m}$  and  $\nu$ . We observe that the onset of the sign problem is delayed as  $\hat{m}$  or  $\nu$  is increased, a feature which is in common with three-colour QCD [46, 50]. In figure 15 we plot the average sign against a rescaled variable  $\hat{\mu}/\sqrt{\hat{m}/2}$ . In physical units, it is equal to  $\mu/(m_\pi/2)$ , where  $m_\pi$  denotes

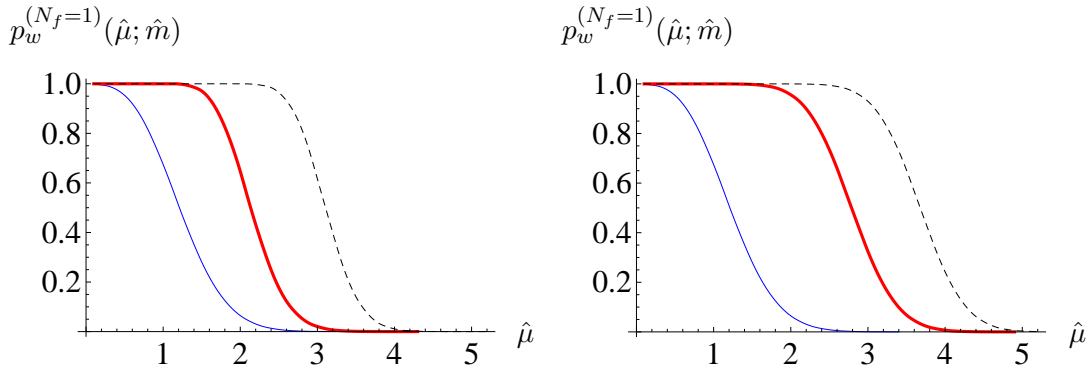


**Figure 14.** Average sign for  $N_f = 1$  at weak non-Hermiticity. Left:  $\hat{m} = 0$  (blue line),  $\hat{m} = 6i$  (red thick line) and  $\hat{m} = 15i$  (black dashed line), all for  $\nu = 0$ . Right:  $\nu = 0$  (blue line),  $\nu = 10$  (red thick line) and  $\nu = 20$  (black dashed line), all for  $\hat{m} = 0$ .

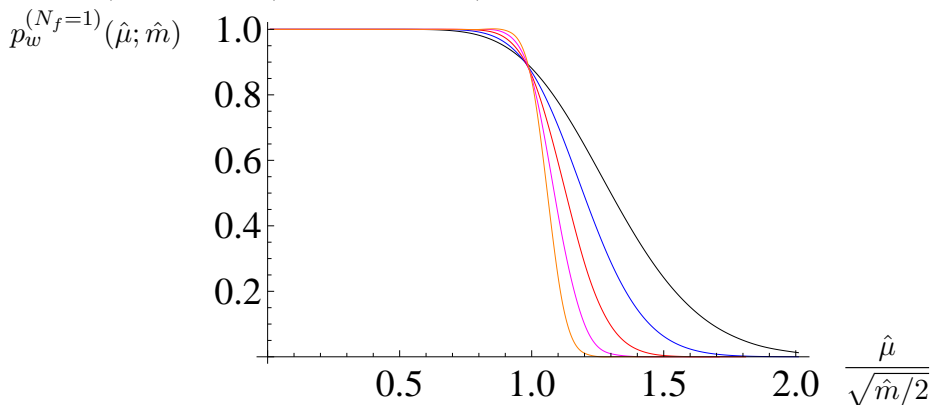


**Figure 15.** Average sign for  $N_f = 1$  and  $\nu = 0$  at weak non-Hermiticity. The curves correspond to  $\hat{m} = 4i$  (black),  $\hat{m} = 8i$  (blue),  $\hat{m} = 16i$  (red),  $\hat{m} = 32i$  (magenta), and  $\hat{m} = 64i$  (orange).

the mass of the Nambu-Goldstone (NG) bosons in the vacuum.<sup>9</sup> Interestingly, the sign problem looks almost absent for  $\mu < m_\pi/2$  while it deteriorates rapidly for  $\mu > m_\pi/2$ . In particular, we observe a convergence of the curves to a step function in the thermodynamic limit. This apparent jump of the average sign is quite intriguing, compared to the average phase factor in the microscopic limit of three-colour QCD [46, 47]: the latter changes smoothly from 1 to 0 in the limit  $\hat{m} \rightarrow \infty$ .

Since the  $\hat{\mu}$ -dependence of  $\mathcal{Z}_w^{(N_f=1, \nu)}$  is explicit in eq. (2.15) (being of oscillatory nature, see eq. (2.9)), it must be  $\mathcal{Z}_w^{(N_f=\|1\|, \nu)}$  that is responsible for the apparent jump of the average sign. While it seems that the  $N_f = \|1\|$  theory is similar to the  $N_f \geq 2$  theory in that both undergo a transition at  $\mu = m_\pi/2$ , see, e.g., [9], a comparison of the order of the transition needs further investigation.

Finally we comment on a lattice simulation using one flavour of staggered fermions in the adjoint representation of  $SU(2)$  [7, 8]. This theory belongs to the same symmetry class as  $N_f = 1$  two-colour QCD with fundamental fermions. In [7, 8] this theory was simulated by two different algorithms, Hybrid-Monte-Carlo (HMC) and Two-Step-Multi-

<sup>9</sup>Note that no NG mode appears in  $N_f = 1$  two-colour QCD. The above  $m_\pi$  refers to the mass of the NG modes that appear in  $N_f \geq 2$  two-colour QCD.

Boson (TSMB). The HMC algorithm is non-ergodic in this case and actually simulates a different theory, namely the one-flavour sign-quenched theory. The authors of [7, 8] report that the sign-quenched theory simulated by HMC seems to undergo a phase transition at  $\mu = m_\pi/2$ , while the correct one-flavour theory simulated by TSMB exhibits no singularity at all. These results are consistent with ours. However, the observables considered here and in [7, 8] are different so that a direct comparison is difficult.

### 4.2.3 Average sign at high density

Let us now consider the case  $N_f = 2$  in the limit of strong non-Hermiticity. This theory is free from the sign problem if and only if the masses are degenerate. Here we are interested in the severity of the sign problem for  $|\hat{m}_1 - \hat{m}_2|$  nonzero. In appendix C.4 we derive

$$\begin{aligned} \mathcal{Z}_s^{(N_f=2, \nu)}(\mu; \hat{m}_1, \hat{m}_2) &\equiv \lim_{N \rightarrow \infty, \text{strong}} \left\langle \left| \det[\mathcal{D}(\mu) + m_1] \det[\mathcal{D}(\mu) + m_2] \right| \right\rangle_{N_f=0} \\ &\sim \frac{f_s(\hat{m}_1^2, \hat{m}_2^2)}{|\hat{m}_1^2 - \hat{m}_2^2|}, \end{aligned} \quad (4.25)$$

where<sup>10</sup>

$$\begin{aligned} f_s(\hat{m}_1^2, \hat{m}_2^2) &= \mathcal{K}_s(\hat{m}_1^2, \hat{m}_2^2) \operatorname{sgn}(\hat{m}_1^2 - \hat{m}_2^2) \\ &+ \int_{\mathbb{R}} dx \int_{\mathbb{R}} dx' \hat{h}_s(x) \hat{h}_s(x') \left[ \operatorname{sgn}(\hat{m}_1^2 - x) \operatorname{sgn}(\hat{m}_2^2 - x') - \operatorname{sgn}(\hat{m}_2^2 - x) \operatorname{sgn}(\hat{m}_1^2 - x') \right] \\ &\quad \times \left[ \mathcal{K}_s(\hat{m}_1^2, x) \mathcal{K}_s(\hat{m}_2^2, x') - \frac{1}{2} \mathcal{K}_s(\hat{m}_1^2, \hat{m}_2^2) \mathcal{K}_s(x, x') \right] \end{aligned} \quad (4.26)$$

with the kernel in the strong limit from eq. (2.10),

$$\mathcal{K}_s(u, v) \equiv \frac{\eta_+^3}{8\pi} (u - v) e^{-\eta_-(u+v)} I_\nu(2\eta_+ \sqrt{uv}). \quad (4.27)$$

These results are obtained from the two-point correlation function of real eigenvalues in the strong limit. Combining eq. (4.25) with eq. (2.14),

$$\mathcal{Z}_s^{(N_f=2, \nu)}(\mu; \hat{m}_1, \hat{m}_2) \sim \frac{\mathcal{K}_s(\hat{m}_1^2, \hat{m}_2^2)}{\hat{m}_1^2 - \hat{m}_2^2},$$

we obtain

$$p_s^{(N_f=2)}(\mu; \hat{m}_1, \hat{m}_2) = \frac{\mathcal{Z}_s^{(N_f=2, \nu)}(\mu; \hat{m}_1, \hat{m}_2)}{\mathcal{Z}_s^{(N_f=2, \nu)}(\mu; \hat{m}_1, \hat{m}_2)} = \operatorname{sgn}(\hat{m}_1^2 - \hat{m}_2^2) \frac{\mathcal{K}_s(\hat{m}_1^2, \hat{m}_2^2)}{f_s(\hat{m}_1^2, \hat{m}_2^2)}. \quad (4.28)$$

This expression satisfies the normalisation condition  $\lim_{\hat{m}_2 \rightarrow \hat{m}_1} p_s^{(N_f=2)}(\mu; \hat{m}_1, \hat{m}_2) = 1$ . By explicit calculation a scaling law is verified,

$$p_s^{(N_f=2)}(\mu; \hat{m}_1, \hat{m}_2) = p_s^{(N_f=2)}(1; \sqrt{2\eta_+} \hat{m}_1, \sqrt{2\eta_+} \hat{m}_2), \quad (4.29)$$

<sup>10</sup>In eq. (4.26) the squared masses are assumed to be nonpositive since this is the case relevant for two-colour QCD. If one or both of the arguments of  $f_s$  are positive we obtain a more complicated expression for  $f_s(x_1, x_2) = \lim_{N \rightarrow \infty} (x_1 x_2)^{\nu/2} f_N(x_1, x_2)$ .

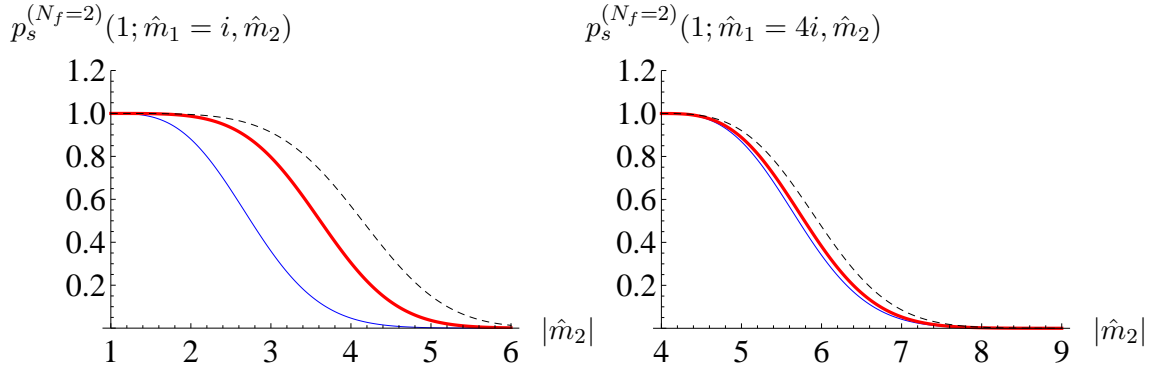


**Figure 16.** Average sign factor for  $N_f = 2$  at maximal non-Hermiticity ( $\hat{\mu} = 1$ ) with  $\hat{m}_1 = i$  (left) and  $\hat{m}_1 = 4i$  (right), at  $\nu = 0$  (blue line),  $\nu = 10$  (red thick line), and  $\nu = 20$  (black dashed line).

hence we can assume  $\mu = 1$  without loss of generality.

In figure 16 we plot  $p_s^{(N_f=2)}(1; \hat{m}_1, \hat{m}_2)$  as a function of  $\hat{m}_2$ . The results indicate that larger topology mitigates the sign problem but becomes less effective for heavier masses. This phenomenon is easily understood if one recalls that a large  $\nu$  that causes a depletion of eigenvalues near the origin can smoothen the strongly oscillating domain of the spectrum if the domain is close to the origin; since the domain moves away from the origin for heavier masses, the smoothing by  $\nu$  becomes less effective.

As a result, the average sign turns out to be essentially independent of topology for larger masses, where the sign problem becomes severe for  $|\delta\hat{m}| \gtrsim 2.5$ , as can also be seen from figure 16. In physical units we have, using eq. (2.6),

$$|\delta m_{\text{phys}}| \gtrsim \frac{4.5}{\sqrt{V_4 \Delta^2}}. \quad (4.30)$$

We remark that the oscillations of the complex spectral density start if  $|\delta\hat{m}| \gtrsim \sqrt{2\pi} \approx 2.5$  as seen from eq. (4.13) at  $\hat{\mu} = 1$ . It is reasonable that these two values of  $|\delta\hat{m}|$  are close to each other.

## 5 Conclusions

In this paper we have solved a random two-matrix model as a mathematical model for unquenched two-colour QCD with non-vanishing chemical potential. Our model has very interesting features. First of all it describes two very different physical situations, at low and at high density, in the approximation of a static chiral Lagrangian. Despite the sign problem the unquenched random two-matrix model can be solved exactly, and the Dirac operator has very distinct real, imaginary, and complex eigenvalue densities. The sign problem can be switched off or on at fixed chemical potential by tuning, say, the masses of two quark flavours to be degenerate or distinct.

We have given many explicit examples for the various spectral densities for  $N_f = 1, 2$  and 4 flavours and have shown how they behave quantitatively differently when the sign problem is switched on.

We have also introduced a measure for the severity of the sign problem and have analysed the envelope, amplitude, number, and frequency of the oscillations of the spectral density once it becomes negative.

It would be very interesting to compare the predictions we have made with ab initio lattice computations, in both settings of low and high density. There are some remarks to be made for this symmetry class, however. At zero chemical potential two-colour QCD has a substantial probability to have small or zero Dirac operator eigenvalues, which is in contrast to other QCD (-like) theories. Therefore it may be very difficult to reach small enough masses (that make the inversion of the Dirac determinant difficult) in order to see the effect of unquenching in the low-lying spectrum.

The chemical potential introduces an extra repulsion of the spectral density from the origin, which might actually help in this situation. The sign problem on the other hand could be kept under control if the non-degeneracy of the quark masses is kept sufficiently small.

## Acknowledgments

We would like to thank K. Splittorff for fruitful discussions and a critical reading of the manuscript, and J. Bloch for helping us in eliminating typos in some equations. The following financial support is acknowledged: GA thanks the Niels Bohr Foundation as well as the Niels Bohr Institute and International Academy where part of this work was done, TK is supported by the Japan Society for the Promotion of Science for Young Scientists, MJP by an EPSRC doctoral training grant, and TW by DFG through SFB/TR-55.

## A The weakly non-Hermitian limit of the real eigenvalue density

### A.1 Initial steps

In this appendix, we consider the large- $N$  limit at weak non-Hermiticity of the real eigenvalue density for the quenched case, which was not analytically determined in section 4.4 of [34]. The real density of Wishart eigenvalues for finite matrix of “size”  $N$  (where  $N$  is even) and topology  $\nu$  is given by (see section 4.2 of [34])

$$R_{1,N}^{\mathbb{R}}(x) = -G_N(x, x; \mu), \quad (\text{A.1})$$

where

$$\begin{aligned} G_N(x, x'; \mu) &\equiv - \int_{-\infty}^{\infty} dy \operatorname{sgn}(x' - y) h(x') h(y) \mathcal{K}_N(x, y) \\ &= - \int_{-\infty}^{\infty} dy \operatorname{sgn}(x' - y) |x'y|^{\nu/2} e^{\eta - (x'+y)} 2K_{\frac{\nu}{2}}(\eta_+ |x'|) 2K_{\frac{\nu}{2}}(\eta_+ |y|) \mathcal{K}_N(x, y) \end{aligned} \quad (\text{A.2})$$

and the quenched kernel at finite  $N$  under the integral is given by

$$\begin{aligned} \mathcal{K}_N(x, y) \equiv & \frac{\eta_-}{8\pi(4\mu^2\eta_+)^{\nu+1}} \sum_{j=0}^{N-2} \left(\frac{\eta_-}{\eta_+}\right)^{2j} \frac{(j+1)!}{(j+\nu)!} \\ & \times \left\{ L_{j+1}^\nu \left(\frac{y}{4\mu^2\eta_-}\right) L_j^\nu \left(\frac{x}{4\mu^2\eta_-}\right) - L_{j+1}^\nu \left(\frac{x}{4\mu^2\eta_-}\right) L_j^\nu \left(\frac{y}{4\mu^2\eta_-}\right) \right\}. \end{aligned} \quad (\text{A.3})$$

For completeness we also give here the even skew-orthogonal polynomials since they appear in their limiting form in eq. (2.9),

$$q_{2k}(z) \equiv (4\mu^2\eta_-)^{2k} (2k)! L_{2k}^\nu \left(\frac{z}{4\mu^2\eta_-}\right). \quad (\text{A.4})$$

We now define the weakly non-Hermitian large- $N$  limit by

$$G_w(x, x'; \hat{\mu}) \equiv \lim_{N \rightarrow \infty} \frac{1}{4N} \frac{x^{\nu/2}}{(x')^{\nu/2}} G_N \left(\frac{x}{4N}, \frac{x'}{4N}; \frac{\hat{\mu}}{\sqrt{2N}}\right). \quad (\text{A.5})$$

The problem is that the limit in eq. (A.5) and the integral in eq. (A.2) do not commute. Using the fact that

$$\int_{-\infty}^{\infty} dy \operatorname{sgn}(x' - y) f(y) = \left( \int_{-\infty}^0 dy + 2 \int_0^{x'} dy - \int_0^{\infty} dy \right) f(y) \quad (\text{A.6})$$

we can correspondingly write  $G_w(x, x'; \hat{\mu})$  as the sum of three parts,

$$G_w(x, x'; \hat{\mu}) = -\{A(x, x'; \hat{\mu}) + 2B(x, x'; \hat{\mu}) - C(x, x'; \hat{\mu})\}. \quad (\text{A.7})$$

For  $A$  and  $B$ , it is possible to interchange the limit and the integral, and so we have simply

$$A(x, x'; \hat{\mu}) = (-i)^\nu \frac{\hat{h}_w(x')}{[\operatorname{sgn}(x')]^{\nu/2}} \int_{-\infty}^0 dy \mathcal{K}_w(x, y) \hat{h}_w(y), \quad (\text{A.8})$$

$$B(x, x'; \hat{\mu}) = \frac{\hat{h}_w(x')}{[\operatorname{sgn}(x')]^\nu} \int_0^{x'} dy \mathcal{K}_w(x, y) \hat{h}_w(y), \quad (\text{A.9})$$

where the scaled weight function and the weak kernel are given by eqs. (3.17) and (2.8), respectively,

$$\begin{aligned} \hat{h}_w(x) &= e^{x/8\hat{\mu}^2} 2K_{\frac{\nu}{2}} \left(\frac{|x|}{8\hat{\mu}^2}\right), \\ \mathcal{K}_w(x, y) &= \frac{1}{256\pi\hat{\mu}^2} \int_0^1 ds s^2 e^{-2\hat{\mu}^2 s^2} \left\{ \sqrt{x} J_{\nu+1}(s\sqrt{x}) J_\nu(s\sqrt{y}) - \sqrt{y} J_{\nu+1}(s\sqrt{y}) J_\nu(s\sqrt{x}) \right\}. \end{aligned}$$

The main problem is then reduced to determining  $C(x, x'; \hat{\mu})$ , where the non-commutativity issue remains.

Let us next perform some fairly straightforward manipulation of  $C(x, x'; \hat{\mu})$ . We can immediately take  $N \rightarrow \infty$  for all the  $N$ -dependent factors that lie outside both the integral and the sum. Therefore

$$C(x, x'; \hat{\mu}) = \frac{1}{32\pi\hat{\mu}^2} \frac{\hat{h}_w(x')}{[\operatorname{sgn}(x')]^{\nu/2}} x^{\nu/2} \lim_{N \rightarrow \infty} D_N(x; \hat{\mu}), \quad (\text{A.10})$$

where

$$D_N(x; \hat{\mu}) \equiv \frac{1}{(4N)^{2+\nu}} \int_0^\infty dy \exp\left(\frac{(1 - \frac{\hat{\mu}^2}{2N})y}{8\hat{\mu}^2}\right) K_{\frac{\nu}{2}}\left(\frac{(1 + \frac{\hat{\mu}^2}{2N})y}{8\hat{\mu}^2}\right) |y|^{\nu/2} \quad (\text{A.11})$$

$$\times \sum_{j=0}^{N-2} \left(\frac{1 - \frac{\hat{\mu}^2}{2N}}{1 + \frac{\hat{\mu}^2}{2N}}\right)^{2j} \frac{j!}{(j + \nu)!} \left\{ x L_j^{\nu+1}\left(\frac{x}{4N(1 - \frac{\hat{\mu}^2}{2N})}\right) L_j^\nu\left(\frac{y}{4N(1 - \frac{\hat{\mu}^2}{2N})}\right) - (x \leftrightarrow y) \right\}.$$

Since  $N$  is finite, we can switch the integral and the sum. We will also split the two terms in the curly brackets, writing  $D_N(x; \hat{\mu}) = D_N^+(x; \hat{\mu}) - D_N^-(x; \hat{\mu})$ , where

$$D_N^+(x; \hat{\mu}) \equiv \frac{1}{(4N)^{2+\nu}} \sum_{j=0}^{N-2} \left(\frac{1 - \frac{\hat{\mu}^2}{2N}}{1 + \frac{\hat{\mu}^2}{2N}}\right)^{2j} \frac{j!}{(j + \nu)!} x L_j^{\nu+1}\left(\frac{x}{4N(1 - \frac{\hat{\mu}^2}{2N})}\right) P(j, N, \hat{\mu}) \quad (\text{A.12})$$

with

$$P(j, N, \hat{\mu}) \equiv \int_0^\infty dy \exp\left(\frac{(1 - \frac{\hat{\mu}^2}{2N})y}{8\hat{\mu}^2}\right) K_{\frac{\nu}{2}}\left(\frac{(1 + \frac{\hat{\mu}^2}{2N})y}{8\hat{\mu}^2}\right) L_j^\nu\left(\frac{y}{4N(1 - \frac{\hat{\mu}^2}{2N})}\right) y^{\nu/2} \quad (\text{A.13})$$

and

$$D_N^-(x; \hat{\mu}) \equiv \frac{1}{(4N)^{2+\nu}} \sum_{j=0}^{N-2} \left(\frac{1 - \frac{\hat{\mu}^2}{2N}}{1 + \frac{\hat{\mu}^2}{2N}}\right)^{2j} \frac{j!}{(j + \nu)!} L_j^\nu\left(\frac{x}{4N(1 - \frac{\hat{\mu}^2}{2N})}\right) Q(j, N, \hat{\mu}) \quad (\text{A.14})$$

with

$$Q(j, N, \hat{\mu}) \equiv \int_0^\infty dy \exp\left(\frac{(1 - \frac{\hat{\mu}^2}{2N})y}{8\hat{\mu}^2}\right) K_{\frac{\nu}{2}}\left(\frac{(1 + \frac{\hat{\mu}^2}{2N})y}{8\hat{\mu}^2}\right) L_j^{\nu+1}\left(\frac{y}{4N(1 - \frac{\hat{\mu}^2}{2N})}\right) y^{\nu/2+1}. \quad (\text{A.15})$$

## A.2 Solution for limit of $D_N(x; \hat{\mu})$

Our plan is to try to evaluate the large- $N$  limits of eqs. (A.12) and (A.14) in a manner similar to the way we calculated the weak kernel in section 4.4 of [34]. This involves taking the limit for large  $j$  and  $N$ , with  $j = tN$  and  $t \in [0, 1]$ , of each of the factors inside the sums in eqs. (A.12) and (A.14), and replacing the sums with integrals. So, in the present case, our primary task will be to determine appropriate large- $N$  limits of  $P(j, N, \hat{\mu})$  and  $Q(j, N, \hat{\mu})$ .

It turns out that for  $D_N^+(x; \hat{\mu})$ , this method works in a relatively straightforward manner. However, for  $D_N^-(x; \hat{\mu})$ , we also find an extra contribution that does not involve an integral. This arises from a different large- $N$  scaling of  $Q(j, N, \hat{\mu})$ .

### A.2.1 Determination of limits of $P(j, N, \hat{\mu})$ and $D_N^+(x; \hat{\mu})$

Let us start with eq. (A.13). First, we use [51, eq. (8.432.3)] to replace the modified Bessel function of the second kind with an integral, giving

$$P(j, N, \hat{\mu}) = \frac{\sqrt{\pi}}{\Gamma(\frac{\nu+1}{2})} \left(\frac{1 + \frac{\hat{\mu}^2}{2N}}{16\hat{\mu}^2}\right)^{\nu/2} \int_0^\infty dy \int_1^\infty du (u^2 - 1)^{(\nu-1)/2} e^{-by} L_j^\nu\left(\frac{y}{c}\right) y^\nu \quad (\text{A.16})$$

with

$$b \equiv \frac{1}{8} \left( \frac{u-1}{\hat{\mu}^2} + \frac{u+1}{2N} \right) \quad \text{and} \quad c \equiv 4N \left( 1 - \frac{\hat{\mu}^2}{2N} \right). \quad (\text{A.17})$$

After writing the Laguerre function explicitly as a polynomial, we interchange the order of integrations and perform the integral over  $y$ . The resulting sum can be recombined into a binomial as follows,

$$\begin{aligned} P(j, N, \hat{\mu}) &= \frac{\sqrt{\pi}}{\Gamma\left(\frac{\nu+1}{2}\right)} \left( \frac{1 + \frac{\hat{\mu}^2}{2N}}{16\hat{\mu}^2} \right)^{\nu/2} \frac{(-1)^j (j+\nu)!}{j! c^j} \int_1^\infty du (u^2 - 1)^{(\nu-1)/2} \frac{(1-bc)^j}{b^{j+\nu+1}} \\ &= \frac{2^{\nu+3} \hat{\mu}^{\nu+2} \sqrt{\pi}}{\Gamma\left(\frac{\nu+1}{2}\right)} \frac{(j+\nu)!}{j!} \frac{\left(1 + \frac{\hat{\mu}^2}{2N}\right)^{\nu/2}}{\left(1 - \frac{\hat{\mu}^2}{2N}\right)^j} \int_1^\infty du \frac{(u+1)^{(\nu-1)/2}}{(u-1)^{(\nu+3)/2}} \frac{\left(1 - \frac{\hat{\mu}^2}{N(u-1)} - \frac{\hat{\mu}^4(u+1)}{4N^2(u-1)}\right)^j}{\left(1 + \frac{\hat{\mu}^2}{2N} \frac{(u+1)}{(u-1)}\right)^{j+\nu+1}}. \end{aligned} \quad (\text{A.18})$$

We now wish to set  $j = tN$ , and take the large- $N$  limit whilst keeping  $t$  fixed. In fact,  $j$  should remain an integer, so we will set  $j = [tN]$ , where the square brackets denote the integer part.

In order to take the limit, it is necessary to split  $P(j, N, \hat{\mu})$  into two parts,  $P_1(j, N, \hat{\mu})$ , where the integral runs over  $1 \leq u < 1 + \hat{\mu}^2/N$ , and  $P_2(j, N, \hat{\mu})$ , where the integral is over the range  $1 + \hat{\mu}^2/N \leq u < \infty$ . For  $P_1(j, N, \hat{\mu})$ , we write  $u + 1 = 2 + \mathcal{O}(N^{-1})$ , and then make a change of variables to

$$s = 1 - \frac{\hat{\mu}^2}{N(u-1)} \quad (\text{A.19})$$

with the result that (dropping the  $\mathcal{O}(N^{-1})$  which will vanish when the limit is taken)

$$\int_1^{1+\hat{\mu}^2/N} du \dots = \frac{(-1)^j 2^{(\nu-1)/2} N^{(\nu+1)/2}}{\hat{\mu}^{\nu+1}} \int_0^\infty ds \frac{s^j (1+s)^{(\nu-1)/2}}{(2+s)^{j+\nu+1}} \left(1 - \frac{\hat{\mu}^2(1-s)}{2Ns}\right)^j. \quad (\text{A.20})$$

It is important to note that the overall sign depends on whether  $j$  is an even or an odd integer. This implies that no single limit of  $P_1(j, N, \hat{\mu})$  will exist. To evaluate the integral on the right-hand side of eq. (A.20), we change variables to  $u = j/s$ , leading to

$$\int_0^\infty ds \dots = \frac{1}{j^{(\nu+1)/2}} \int_0^\infty du \left\{ j^{(\nu+3)/2} \frac{u^{(\nu-1)/2} (u+j)^{(\nu-1)/2}}{(2u+j)^{\nu+1} \left(1 + \frac{2u}{j}\right)^j} \left(1 - \frac{\hat{\mu}^2(u-j)}{2Nj}\right)^j \right\}. \quad (\text{A.21})$$

In fact, we are only interested in the large- $N$  limit of this integral, with  $j = [tN]$  and  $t$  fixed. As  $N \rightarrow \infty$ , the integrand in the curly brackets converges to an integrable function in a manner that allows us to interchange the limit and the integral. Therefore

$$\lim_{\substack{N \rightarrow \infty \\ j=[tN]}} j^{(\nu+1)/2} \int_0^\infty ds \dots = e^{\hat{\mu}^2 t} \int_0^\infty du u^{(\nu-1)/2} e^{-2u} = \frac{\Gamma\left(\frac{\nu+1}{2}\right)}{2^{(\nu+1)/2}} e^{\hat{\mu}^2 t}. \quad (\text{A.22})$$

Combining everything, we have

$$\lim_{\substack{N \rightarrow \infty \\ j=[tN]}} \frac{P_1(j, N, \hat{\mu})}{N^\nu} = (-1)^j 2^{\nu+2} \sqrt{\pi} \hat{\mu} t^{(\nu-1)/2} e^{\hat{\mu}^2 t}. \quad (\text{A.23})$$

Note that we have been somewhat imprecise with our notation; there are actually two limits, depending on whether  $j$  steps through the even or the odd integers.

We now turn to consider the limit of  $P_2(j, N, \hat{\mu})$ , for which we can write

$$\int_{1+\hat{\mu}^2/N}^{\infty} du \cdots = \int_1^{\infty} du \Theta \left[ u - \left( 1 + \frac{\hat{\mu}^2}{N} \right) \right] \cdots, \quad (\text{A.24})$$

where  $\Theta(x)$  is the Heaviside step function. We can then use the Monotone Convergence Theorem to show that

$$\begin{aligned} \lim_{\substack{N \rightarrow \infty \\ j=[tN]}} \frac{P_2(j, N, \hat{\mu})}{N^\nu} &= \frac{2^{\nu+3} \sqrt{\pi} \hat{\mu}^{\nu+2} t^\nu}{\Gamma\left(\frac{\nu+1}{2}\right)} \int_1^{\infty} du \frac{(u+1)^{(\nu-1)/2}}{(u-1)^{(\nu+3)/2}} \exp\left[-\frac{2\hat{\mu}^2 t}{u-1}\right] \\ &= \frac{(2\hat{\mu})^{\nu+2} \sqrt{\pi}}{\Gamma\left(\frac{\nu+1}{2}\right)} t^\nu e^{\hat{\mu}^2 t} E_{\frac{1-\nu}{2}}(\hat{\mu}^2 t), \end{aligned} \quad (\text{A.25})$$

where we used a simple change of variables  $s = (u+1)/(u-1)$  in the last step, and  $E_n(x)$  is the exponential integral defined in eq. (3.18). Our formula for the limit of  $P(j, N, \hat{\mu})$  is therefore

$$\lim_{\substack{N \rightarrow \infty \\ j=[tN]}} \frac{P(j, N, \hat{\mu})}{N^\nu} = 2^{\nu+2} \sqrt{\pi} e^{\hat{\mu}^2 t} \left\{ \frac{\hat{\mu}^{\nu+2} t^\nu E_{\frac{1-\nu}{2}}(\hat{\mu}^2 t)}{\Gamma\left(\frac{\nu+1}{2}\right)} + (-1)^j \hat{\mu} t^{(\nu-1)/2} \right\}, \quad (\text{A.26})$$

where it should be understood that there are different limits depending on whether  $j$  takes even or odd values.

Let us now consider the limit of  $D_N^+(x; \hat{\mu})$ . Because of the two different limits of  $P(j, N, \hat{\mu})$ , technically we should now split the sum in eq. (A.12) into odd and even parts, and treat each part separately. However, because of the way that everything combines, it is completely equivalent if we merely use the ‘‘average’’ limit over even and odd  $j$ ,

$$\left\langle \lim_{\substack{N \rightarrow \infty \\ j=[tN]}} \frac{P(j, N, \hat{\mu})}{N^\nu} \right\rangle = \frac{2^{\nu+2} \sqrt{\pi}}{\Gamma\left(\frac{\nu+1}{2}\right)} e^{\hat{\mu}^2 t} \hat{\mu}^{\nu+2} t^\nu E_{\frac{1-\nu}{2}}(\hat{\mu}^2 t), \quad (\text{A.27})$$

where it should be understood that this is the average limit over a small interval around  $t$  which includes (an infinite number of) both even and odd terms in  $j$ .

We can now proceed as in [34],

$$\lim_{N \rightarrow \infty} \sum_{j=0}^{N-2} \frac{1}{N} = \int_0^1 dt, \quad (\text{A.28})$$

$$\lim_{\substack{N \rightarrow \infty \\ j=[tN]}} \left( \frac{1 - \frac{\hat{\mu}^2}{2N}}{1 + \frac{\hat{\mu}^2}{2N}} \right)^{2j} = \exp[-2\hat{\mu}^2 t], \quad (\text{A.29})$$

$$\lim_{\substack{N \rightarrow \infty \\ j=[tN]}} \frac{j!}{(j+\nu)!} N^\nu = t^{-\nu}, \quad (\text{A.30})$$

$$\begin{aligned} \lim_{\substack{N \rightarrow \infty \\ j=[tN]}} \frac{1}{N^{\nu+1}} L_j^{\nu+1} \left( \frac{x}{4N(1 - \frac{\hat{\mu}^2}{2N})} \right) &= \lim_{N \rightarrow \infty} \frac{1}{N^{\nu+1}} L_{[tN]}^{\nu+1} \left( \frac{x}{4N} \right) \\ &= \left( \frac{2\sqrt{t}}{\sqrt{x}} \right)^{\nu+1} J_{\nu+1}(\sqrt{xt}). \end{aligned} \quad (\text{A.31})$$

Hence

$$\lim_{N \rightarrow \infty} D_N^+(x; \hat{\mu}) = \frac{\sqrt{\pi}}{2\Gamma\left(\frac{\nu+1}{2}\right)} \frac{\sqrt{x}}{x^{\nu/2}} \hat{\mu}^{\nu+2} \int_0^1 dt e^{-\hat{\mu}^2 t} t^{(\nu+1)/2} E_{\frac{1-\nu}{2}}(\hat{\mu}^2 t) J_{\nu+1}(\sqrt{xt}). \quad (\text{A.32})$$

### A.2.2 Determination of limits of $Q(j, N, \hat{\mu})$ and $D_N^-(x; \hat{\mu})$

For  $Q(j, N, \hat{\mu})$ , we find that we expect the limit

$$\lim_{\substack{N \rightarrow \infty \\ j=[tN]}} \frac{Q(j, N, \hat{\mu})}{N^{\nu+2}} \quad (\text{A.33})$$

to exist. The key point is that there are *two* powers of  $N$  difference compared with the  $P(j, N, \hat{\mu})$  case, which we can see as follows. Using the recurrence relation [51, eq. (8.971.4)]

$$z L_j^{\nu+1}(z) = (j+1) \left\{ L_j^{\nu}(z) - L_{j+1}^{\nu}(z) \right\} + L_j^{\nu}(z) \quad (\text{A.34})$$

we can show that

$$\frac{Q(j, N, \hat{\mu})}{N} = 4 \left( 1 - \frac{\hat{\mu}^2}{2N} \right) \left[ (j+1) \left\{ P(j, N, \hat{\mu}) - P(j+1, N, \hat{\mu}) \right\} + \nu P(j, N, \hat{\mu}) \right]. \quad (\text{A.35})$$

Since  $j+1 \propto N$  at large  $N$ , there are two powers of  $N$  difference between the leading orders of  $P$  and  $Q$ , and not one, as might naïvely have been expected.

**Leading order contribution:** We use eqs. (A.26) and (A.35) to show that

$$\lim_{\substack{N \rightarrow \infty \\ j=[tN]}} \frac{Q(j, N, \hat{\mu})}{N^{\nu+2}} = (-1)^j 2^{\nu+5} \sqrt{\pi} \hat{\mu} t^{(\nu+1)/2} e^{\hat{\mu}^2 t}, \quad (\text{A.36})$$

where the sign depends on whether  $j$  is even or odd. Note that the other terms from eqs. (A.26) and (A.35) are of smaller order, and so will vanish in the large- $N$  limit.

Now let us consider the limit of  $D_N^-(x; \hat{\mu})$ . The presence of the  $N^{\nu+2}$  scaling for  $Q$  is the crucial difference compared with the  $P$  case, which scaled only with  $N^{\nu}$ . Although the  $N^{\nu+2}$  here can be matched with the  $N^{\nu+2}$  prefactor in eq. (A.14), this means that there is then no residual  $N^{-1}$  to make  $dt$  when we take the large- $N$  limit (see eq. (A.28)), and so we will not get an integral.

Because adjacent even and odd terms have opposite signs, however, we can use the fact that, for a continuous function  $f(t)$  on the interval  $0 \leq t \leq 1$ ,

$$\lim_{N \rightarrow \infty} \sum_{j=0}^{N/2-1} \left\{ f\left(\frac{2j+1}{N}\right) - f\left(\frac{2j}{N}\right) \right\} = \frac{1}{2} \{f(1) - f(0)\} \quad (\text{A.37})$$

to take the large- $N$  limit of the sum in eq. (A.14). This results in a contribution of

$$\lim_{\substack{N \rightarrow \infty \\ \text{Regime 1}}} D_N^-(x; \hat{\mu}) = \frac{\sqrt{\pi}}{x^{\nu/2}} \hat{\mu} \left[ e^{-\hat{\mu}^2 t} \sqrt{t} J_{\nu}(\sqrt{xt}) \right]_{t=0}^{t=1} = \frac{\sqrt{\pi} \hat{\mu} e^{-\hat{\mu}^2}}{x^{\nu/2}} J_{\nu}(\sqrt{x}). \quad (\text{A.38})$$

**Next-to-leading order contribution:** There will also be a contribution from the next-to-leading order term of  $Q$ . Here, we *can* average even and odd terms (as we did for  $P(j, N, \hat{\mu})$  in eq. (A.26)), and this average gives zero for the leading order. So the effective limit (over a small neighbourhood of  $t$ ) is here (from eq. (A.35))

$$\begin{aligned} \left\langle \lim_{\substack{N \rightarrow \infty \\ j=[tN]}} \frac{Q(j, N, \hat{\mu})}{N^{\nu+1}} \right\rangle &= 4 \left( -t \frac{\partial}{\partial t} + \nu \right) \left\langle \lim_{\substack{N \rightarrow \infty \\ j=[tN]}} \frac{P(j, N, \hat{\mu})}{N^\nu} \right\rangle \\ &= \frac{\sqrt{\pi}}{\Gamma\left(\frac{\nu+1}{2}\right)} (2\hat{\mu})^{4+\nu} t^{1+\nu} e^{\hat{\mu}^2 t} \left\{ E_{-\frac{1-\nu}{2}}(\hat{\mu}^2 t) - E_{\frac{1-\nu}{2}}(\hat{\mu}^2 t) \right\}, \end{aligned} \quad (\text{A.39})$$

where we used

$$\frac{d}{dx} E_n(x) = -E_{n-1}(x). \quad (\text{A.40})$$

Hence

$$\lim_{\substack{N \rightarrow \infty \\ \text{Regime 2}}} D_N^-(x; \hat{\mu}) = \frac{\sqrt{\pi} \hat{\mu}^{\nu+4}}{\Gamma\left(\frac{\nu+1}{2}\right)} \frac{1}{x^{\nu/2}} \int_0^1 dt e^{-\hat{\mu}^2 t} t^{1+\nu/2} \left\{ E_{-\frac{1-\nu}{2}}(\hat{\mu}^2 t) - E_{\frac{1-\nu}{2}}(\hat{\mu}^2 t) \right\} J_\nu(\sqrt{x t}). \quad (\text{A.41})$$

We should add that lower orders will not contribute to the integral when we take the large- $N$  limit of the sum in eq. (A.14).

### A.2.3 Final formula

Pulling everything together and simplifying, we have

$$\begin{aligned} C(x, x'; \hat{\mu}) &= \frac{1}{32\sqrt{\pi}} \frac{\hat{h}_w(x')}{[\text{sgn}(x')]^{\nu/2}} \left\{ -\frac{1}{\hat{\mu}} e^{-\hat{\mu}^2} J_\nu(\sqrt{x}) + \frac{\hat{\mu}^\nu}{\Gamma\left(\frac{\nu+1}{2}\right)} \int_0^1 dt e^{-\hat{\mu}^2 t} t^{(\nu+1)/2} \right. \\ &\quad \left. \times \left[ \frac{\sqrt{x}}{2} E_{\frac{1-\nu}{2}}(\hat{\mu}^2 t) J_{\nu+1}(\sqrt{x t}) - \hat{\mu}^2 \sqrt{t} \left( E_{-\frac{1-\nu}{2}}(\hat{\mu}^2 t) - E_{\frac{1-\nu}{2}}(\hat{\mu}^2 t) \right) J_\nu(\sqrt{x t}) \right] \right\}. \end{aligned} \quad (\text{A.42})$$

We then substitute this (after an easy change of variables), together with eqs. (A.8) and (A.9), into eq. (A.7) to give eq. (3.16). The final result, although not obtained in a mathematically rigorous manner, is well supported by numerical checks. Furthermore, we have also verified analytically that, on taking the Hermitian limit  $\hat{\mu} \rightarrow 0$ , our result for the density shows complete agreement with [41].

## B Decoupling of heavy flavours

Looking at the RMT partition function (2.1) – and in fact for any QCD-like theory with or without chemical potential – it is expected that the microscopic spectral density would reduce to that for a fewer number of flavours when one or more of the quark masses were sent to infinity,<sup>11</sup>

$$\rho_w^{(N_f)}(\xi) \xrightarrow{|\hat{m}_1| \rightarrow \infty} \rho_w^{(N_f-1)}(\xi) \xrightarrow{|\hat{m}_2| \rightarrow \infty} \rho_w^{(N_f-2)}(\xi) \dots, \quad (\text{B.1})$$

$$\rho_s^{(N_f)}(\xi) \xrightarrow{|\hat{m}_1|, |\hat{m}_2| \rightarrow \infty} \rho_s^{(N_f-2)}(\xi) \xrightarrow{|\hat{m}_3|, |\hat{m}_4| \rightarrow \infty} \rho_s^{(N_f-4)}(\xi) \dots. \quad (\text{B.2})$$

<sup>11</sup>We recall that the masses are purely imaginary.

We note that an even number of masses must be sent to infinity in the strong limit. The decoupling can easily be seen by numerical methods.

We do not give a full proof. Instead we wish to illustrate the decoupling for

$$\rho_w^{(N_f=2, \mathbb{C})}(\xi) \xrightarrow{|\hat{m}_1| \rightarrow \infty} \rho_w^{(N_f=1, \mathbb{C})}(\xi). \quad (\text{B.3})$$

To show this, we use that the weak kernel  $\mathcal{K}_w$  obeys

$$\mathcal{K}_w(v, \hat{m}^2) = -\mathcal{K}_w(\hat{m}^2, v) \simeq f_w(\hat{m}^2)q_w(v) \quad \text{for } -\hat{m}^2 \gg 1, \quad (\text{B.4})$$

where

$$f_w(\hat{m}^2) \equiv \frac{(2i)^\nu}{256\pi\hat{\mu}^2} e^{-\frac{3}{2}\hat{\mu}^2} I_{\nu+1}(|\hat{m}|). \quad (\text{B.5})$$

Thus, in the limit  $-\hat{m}_1^2 \gg 1$ , eq. (3.20) yields

$$\begin{aligned} \rho_w^{(N_f=2, \mathbb{C})}(\xi; \hat{m}_1, \hat{m}_2) &\simeq \rho_w^{(0, \mathbb{C})}(\xi) + 4|\xi|^2 \hat{g}_w(\xi^{*2}, \xi^2) \\ &\quad \times \frac{\mathcal{K}_w(\xi^2, \hat{m}_2^2) \{q_w(\xi^{*2})f_w(\hat{m}_1^2)\} - \{q_w(\xi^2)f_w(\hat{m}_1^2)\} \mathcal{K}_w(\xi^{*2}, \hat{m}_2^2)}{-f_w(\hat{m}_1^2)q_w(\hat{m}_2^2)} \\ &= \rho_w^{(0, \mathbb{C})}(\xi) + 4|\xi|^2 \hat{g}_w(\xi^{*2}, \xi^2) \frac{-\mathcal{K}_w(\xi^2, \hat{m}_2^2)q_w(\xi^{*2}) + q_w(\xi^2)\mathcal{K}_w(\xi^{*2}, \hat{m}_2^2)}{q_w(\hat{m}_2^2)} \\ &= \rho_w^{(N_f=1, \mathbb{C})}(\xi; \hat{m}_2), \end{aligned} \quad (\text{B.6})$$

as seen from eq. (3.25). These steps can be generalised to higher  $N_f$  in a straightforward manner.

The decoupling occurs in the sectors of real/imaginary eigenvalues as well, as seen in figures 7 and 8. For illustration, let us prove

$$\rho_w^{(N_f=2, (i)\mathbb{R})}(\xi; \hat{m}_1, \hat{m}_2) \xrightarrow{|\hat{m}_1| \rightarrow \infty} \rho_w^{(N_f=1, (i)\mathbb{R})}(\xi; \hat{m}_2). \quad (\text{B.7})$$

With eq. (B.4) it can be proven that

$$G_w(x, x') \xrightarrow{x \rightarrow -\infty} f_w(x)Q_w(x'). \quad (\text{B.8})$$

Using eqs. (B.4) and (B.8) in eq. (3.24), we find, in the limit  $-\hat{m}_1^2 \gg 1$ , that

$$\begin{aligned} &\rho_w^{(N_f=2, (i)\mathbb{R})}(\xi; \hat{m}_1, \hat{m}_2) \\ &\simeq \rho_w^{(0, (i)\mathbb{R})}(\xi) + 2|\xi| \frac{\mathcal{K}_w(\xi^2, \hat{m}_2^2) \{f_w(\hat{m}_1^2)Q_w(\xi^2)\} - \{q_w(\xi^2)f_w(\hat{m}_1^2)\} G_w(\hat{m}_2^2, \xi^2)}{-f_w(\hat{m}_1^2)q_w(\hat{m}_2^2)} \\ &= \rho_w^{(0, (i)\mathbb{R})}(\xi) + 2|\xi| \frac{\mathcal{K}_w(\xi^2, \hat{m}_2^2)Q_w(\xi^2) - q_w(\xi^2)G_w(\hat{m}_2^2, \xi^2)}{-q_w(\hat{m}_2^2)} \\ &= \rho_w^{(N_f=1, (i)\mathbb{R})}(\xi; \hat{m}_2), \end{aligned} \quad (\text{B.9})$$

as seen from eq. (3.26). Moreover using eqs. (B.4) and (B.8) once again we can easily prove  $\rho_w^{(N_f=1, (i)\mathbb{R})}(\xi; \hat{m}_2) \rightarrow \rho_w^{(0, (i)\mathbb{R})}(\xi)$  for  $-\hat{m}_2^2 \gg 1$ .

## C Sign-quenched partition functions

In two-colour QCD the fermion determinant has no complex phase but only a sign, so we shall introduce a “sign-quenched” partition function, in which  $\det[\mathcal{D}(\mu) + \hat{m}]$  is replaced by  $|\det[\mathcal{D}(\mu) + \hat{m}]|$ , as a direct counterpart of the phase-quenched partition function in three-colour QCD. The purpose of this appendix is to derive analytical expressions for such sign-quenched partition functions, first for finite  $N$ , and later in the limits of both weak and strong non-Hermiticity. The results in this appendix will be used in the main text for the analysis of the sign problem.

### C.1 Main result for finite $N$

Let us begin with a formula for the probability measure, with  $z_j \equiv x_j + iy_j$ ,

$$\begin{aligned} \mathcal{Z}_N^{(N_f, \nu)}(\mu; \{m\}) &= c_N \prod_{f=1}^{N_f} m_f^\nu \prod_{k=1}^N \int_{\mathbb{C}} d^2 z_k w(z_k) |\Delta_N(\{z\})| \prod_{j=1}^N \prod_{f=1}^{N_f} (m_f^2 - z_j) \\ &\times \sum_{n=0}^{[N/2]} \frac{1}{n!(N-2n)!} \prod_{i=1}^n \delta^2(z_{2i-1} - z_{2i}^*) \delta(y_{2n+1}) \cdots \delta(y_N), \end{aligned} \quad (\text{C.1})$$

which is a minor modification of [34, eq. (2.9)]. Whilst being equal to eq. (3.3) for even  $N$ , this expression is more convenient for our current purpose. The weight function  $w(z)$  is defined in [34, eq. (2.12)], and below we only use that  $w(z) = w(z^*)$  for  $z \in \mathbb{C}$ , and  $w(z) = h(z)$  for  $z \in \mathbb{R}$ , with  $h(z)$  defined in eq. (3.5). The prefactor  $c_N$  reads

$$c_N \equiv (\mu\text{-independent factor}) \times (2\mu)^{-N(N+\nu)} \eta_+^{-N(N+\nu-1)/2}, \quad (\text{C.2})$$

and we refer to [34, eq. (3.46)] for more details.

We also define a “partially sign-quenched” partition function, which we denote by  $\mathcal{Z}_N^{(\|\tilde{m}\|+N_f, \nu)}(\mu; \{\tilde{m}\}, \{m\})$ , as being identical to  $\mathcal{Z}_N^{(N_f+N_f, \nu)}$  in eq. (C.1) except that the fermion determinant is replaced by

$$\prod_{j=1}^N \left[ \prod_{h=1}^{N'_f} |\tilde{m}_h|^\nu |\tilde{m}_h^2 - z_j| \prod_{f=1}^{N_f} m_f^\nu (m_f^2 - z_j) \right]. \quad (\text{C.3})$$

After these prerequisites, we can now state our main result at finite  $N$ ,

$$R_{k,N}^{(N_f, \mathbb{R})}(x_1, \dots, x_k) = \frac{c_N}{c_{N-k}} |\Delta_k(\{x\})| \prod_{i=1}^k \frac{w(x_i)}{|x_i|^{\nu/2}} \prod_{f=1}^{N_f} (m_f^2 - x_i) \frac{\mathcal{Z}_{N-k}^{(\|k\|+N_f, \nu)}(\mu; \{\sqrt{x}\}, \{m\})}{\mathcal{Z}_N^{(N_f, \nu)}(\mu; \{m\})}. \quad (\text{C.4})$$

Below we give a proof of this formula for  $k = 1$ . The generalization to  $k > 1$  is then straightforward.

## C.2 Proof: the $k = 1$ case

By definition, we have

$$\begin{aligned}
R_{1,N}^{(N_f)}(z) &= \frac{c_N}{\mathcal{Z}_N^{(N_f,\nu)}(\mu; \{m\})} \prod_{f=1}^{N_f} m_f^\nu \prod_{k=1}^N \int_{\mathbb{C}} d^2 z_k w(z_k) |\Delta_N(\{z\})| \prod_{j=1}^N \prod_{f=1}^{N_f} (m_f^2 - z_j) \\
&\times \sum_{n=0}^{[N/2]} \frac{1}{n!(N-2n)!} \prod_{i=1}^n \delta^2(z_{2i-1} - z_{2i}^*) \delta(y_{2n+1}) \cdots \delta(y_N) \sum_{\ell=1}^N \delta^2(z - z_\ell). \quad (\text{C.5})
\end{aligned}$$

For  $2n+1 \leq \ell \leq N$ ,  $\delta^2(z - z_\ell)$  in the last sum will yield  $\delta(y)$  (with  $z \equiv x + iy$ ), hence

$$\begin{aligned}
\delta(y) R_{1,N}^{(N_f,\mathbb{R})}(x) &= \frac{c_N}{\mathcal{Z}_N^{(N_f,\nu)}(\mu; \{m\})} \prod_{f=1}^{N_f} m_f^\nu \prod_{k=1}^N \int_{\mathbb{C}} d^2 z_k w(z_k) |\Delta_N(\{z\})| \prod_{j=1}^N \prod_{f=1}^{N_f} (m_f^2 - z_j) \\
&\times \sum_{n=0}^{[N/2]} \frac{1}{n!(N-2n)!} \prod_{i=1}^n \delta^2(z_{2i-1} - z_{2i}^*) \delta(y_{2n+1}) \cdots \delta(y_N) \sum_{\ell=2n+1}^N \delta^2(z - z_\ell) \\
&= \frac{c_N}{\mathcal{Z}_N^{(N_f,\nu)}(\mu; \{m\})} \prod_{f=1}^{N_f} m_f^\nu \prod_{k=1}^N \int_{\mathbb{C}} d^2 z_k w(z_k) |\Delta_N(\{z\})| \prod_{j=1}^N \prod_{f=1}^{N_f} (m_f^2 - z_j) \\
&\times \sum_{n=0}^{[N/2]} \frac{N-2n}{n!(N-2n)!} \prod_{i=1}^n \delta^2(z_{2i-1} - z_{2i}^*) \delta(y_{2n+1}) \cdots \delta(y_N) \delta^2(z - z_N) \\
&= \frac{c_N}{\mathcal{Z}_N^{(N_f,\nu)}(\mu; \{m\})} w(x) \prod_{f=1}^{N_f} (m_f^2 - x) \prod_{f=1}^{N_f} m_f^\nu \\
&\times \prod_{k=1}^{N-1} \int_{\mathbb{C}} d^2 z_k w(z_k) \left( |\Delta_{N-1}(\{z\})| \prod_{\ell=1}^{N-1} |x - z_\ell| \right) \prod_{j=1}^{N-1} \prod_{f=1}^{N_f} (m_f^2 - z_j) \\
&\times \sum_{n=0}^{[N/2]} \frac{1}{n!(N-1-2n)!} \prod_{i=1}^n \delta^2(z_{2i-1} - z_{2i}^*) \delta(y_{2n+1}) \cdots \delta(y_{N-1}) \delta(y). \quad (\text{C.6})
\end{aligned}$$

Therefore

$$R_{1,N}^{(N_f,\mathbb{R})}(x) = \frac{c_N}{c_{N-1}} \frac{w(x)}{|x|^{\nu/2}} \prod_{f=1}^{N_f} (m_f^2 - x) \frac{\mathcal{Z}_{N-1}^{(\|1\|+N_f,\nu)}(\mu; \sqrt{x}, \{m\})}{\mathcal{Z}_N^{(N_f,\nu)}(\mu; \{m\})}. \quad (\text{C.7})$$

## C.3 The large- $N$ limit of weak non-Hermiticity

Here we shall compute  $\mathcal{Z}^{(N_f=\|1\|,\nu)}(\mu; \{m\}) = \langle |\det[\mathcal{D}(\mu) + m]| \rangle$  in the limit of weak non-Hermiticity defined in eq. (3.11),

$$\begin{aligned}
\hat{\mu}^2 &\equiv 2N\mu^2, \\
\hat{m}_f &\equiv 2\sqrt{N}m_f,
\end{aligned}$$

$$\xi \equiv 2\sqrt{N}\Lambda.$$

Putting  $N_f = 0$  and  $x = m^2 \in \mathbb{R}$  in eq. (C.7), we find

$$\lim_{N \rightarrow \infty} \mathcal{Z}_{N-1}^{(N_f=||1||, \nu)}(\mu; m) \sim \frac{c_{N-1}}{c_N} \frac{|m|^\nu}{w(m^2)} R_{1,N}^{(N_f=0, \mathbb{R})}(m^2). \quad (\text{C.8})$$

In the weak limit, it follows from eqs. (3.10) and (3.15) that

$$\lim_{N \rightarrow \infty} R_{1,N}^{(N_f=0, \mathbb{R})}(m^2) \sim R_w^{(N_f=0, \mathbb{R})}(\hat{m}^2) = -G_w(\hat{m}^2, \hat{m}^2), \quad (\text{C.9})$$

$$\lim_{N \rightarrow \infty} \frac{|m|^\nu}{w(m^2)} \sim \frac{1}{\hat{h}_w(\hat{m}^2)}. \quad (\text{C.10})$$

From eq. (C.2), we have

$$\lim_{N \rightarrow \infty} \frac{c_{N-1}}{c_N} \sim \frac{(2\mu)^{-(N-1)(N-1+\nu)} \eta_+^{-(N-1)(N+\nu-2)/2}}{(2\mu)^{-N(N+\nu)} \eta_+^{-N(N+\nu-1)/2}} = (2\mu)^{2N+\nu-1} \eta_+^{N-1+\nu/2} \quad (\text{C.11})$$

$$\sim \sqrt{2N} \mu e^{N\mu^2} = \hat{\mu} e^{\hat{\mu}^2/2}. \quad (\text{C.12})$$

Collecting all results, we finally obtain eq. (4.23),

$$\mathcal{Z}_w^{(N_f=||1||, \nu)}(\hat{\mu}; \hat{m}) \sim -\hat{\mu} e^{\hat{\mu}^2/2} \frac{G_w(\hat{m}^2, \hat{m}^2)}{\hat{h}_w(\hat{m}^2)}.$$

#### C.4 The large- $N$ limit of strong non-Hermiticity

Below we show how to derive an analytical expression in the limit of strong non-Hermiticity for  $\mathcal{Z}_N^{(N_f=||2||, \nu)}(\mu; m_1, m_2) = \langle |\det[\mathcal{D}(\mu) + m_1] \det[\mathcal{D}(\mu) + m_2]| \rangle$ , where  $N$  goes to infinity with  $\mu$  and  $m_f$  fixed ( $\hat{m}_f = m_f$ ).

Putting  $k = 2$ ,  $N_f = 0$ ,  $x_1 = m_1^2$ , and  $x_2 = m_2^2$  (with  $m_1^2, m_2^2 \in \mathbb{R}$ ) in eq. (C.4) and using  $w(x) = h(x)$  for  $x \in \mathbb{R}$ , we find

$$\mathcal{Z}_{N-2}^{(N_f=||2||, \nu)}(\mu; m_1, m_2) \sim \frac{c_{N-2}}{c_N} \frac{1}{|m_1^2 - m_2^2|} \frac{|m_1 m_2|^\nu}{h(m_1^2) h(m_2^2)} R_{2,N}^{(N_f=0, \mathbb{R})}(m_1^2, m_2^2). \quad (\text{C.13})$$

Next, let us recall that according to [34, 52] the real two-point function reads

$$R_{2,N}^{(N_f=0, \mathbb{R})}(x_1, x_2) = h(x_1) h(x_2) f_N(x_1, x_2), \quad (\text{C.14})$$

where

$$\begin{aligned} f_N(x_1, x_2) &\equiv \mathcal{K}_N(x_1, x_2) \operatorname{sgn}(x_1 - x_2) \\ &+ \int_{\mathbb{R}} dx \int_{\mathbb{R}} dx' h(x) h(x') \left[ \operatorname{sgn}(x_1 - x) \operatorname{sgn}(x_2 - x') - \operatorname{sgn}(x_2 - x) \operatorname{sgn}(x_1 - x') \right] \\ &\quad \times \left[ \mathcal{K}_N(x_1, x) \mathcal{K}_N(x_2, x') - \frac{1}{2} \mathcal{K}_N(x_1, x_2) \mathcal{K}_N(x, x') \right]. \end{aligned} \quad (\text{C.15})$$

We can plug eq. (C.14) into eq. (C.13) to get eq. (4.25),

$$\mathcal{Z}_s^{(N_f=||2||, \nu)}(\mu; \hat{m}_1, \hat{m}_2) \sim \frac{f_s(\hat{m}_1^2, \hat{m}_2^2)}{|\hat{m}_1^2 - \hat{m}_2^2|},$$

where  $f_s(x_1, x_2)$  is defined as the large- $N$  limit of  $(x_1 x_2)^{\nu/2} f_N(x_1, x_2)$ , with no additional rescaling of parameters involved, and is explicitly given in eq. (4.26) for nonpositive arguments. In eq. (4.25) we omitted a  $\mu$ -dependent prefactor on the right-hand side, as our primary interest in the strong limit is in the mass dependence of the quantities considered.

## References

- [1] Y. Aoki *et al.*, *The QCD transition temperature: results with physical masses in the continuum limit II*, *JHEP* **06** (2009) 088, [[arXiv:0903.4155](#)].
- [2] P. de Forcrand, *Simulating QCD at finite density*, *PoS LAT2009* (2009) 010, [[arXiv:1005.0539](#)].
- [3] M. G. Alford, A. Schmitt, K. Rajagopal, and T. Schäfer, *Color superconductivity in dense quark matter*, *Rev. Mod. Phys.* **80** (2008) 1455–1515, [[arXiv:0709.4635](#)].
- [4] R. Rapp, T. Schafer, E. V. Shuryak, and M. Velkovsky, *High-density QCD and instantons*, *Annals Phys.* **280** (2000) 35–99, [[hep-ph/9904353](#)].
- [5] K. Fukushima, *Phase diagrams in the three-flavor Nambu–Jona-Lasinio model with the Polyakov loop*, *Phys. Rev.* **D77** (2008) 114028, [[arXiv:0803.3318](#)].
- [6] A. M. Halasz, A. D. Jackson, R. E. Shrock, M. A. Stephanov, and J. J. M. Verbaarschot, *On the phase diagram of QCD*, *Phys. Rev.* **D58** (1998) 096007, [[hep-ph/9804290](#)].
- [7] S. Hands *et al.*, *Numerical study of dense adjoint matter in two color QCD*, *Eur. Phys. J.* **C17** (2000) 285–302, [[hep-lat/0006018](#)].
- [8] S. Hands, I. Montvay, L. Scorzato, and J. Skullerud, *Diquark condensation in dense adjoint matter*, *Eur. Phys. J.* **C22** (2001) 451–461, [[hep-lat/0109029](#)].
- [9] J. B. Kogut, M. A. Stephanov, D. Toublan, J. J. M. Verbaarschot, and A. Zhitnitsky, *QCD-like theories at finite baryon density*, *Nucl. Phys.* **B582** (2000) 477–513, [[hep-ph/0001171](#)].
- [10] J. B. Kogut, D. K. Sinclair, S. J. Hands, and S. E. Morrison, *Two-colour QCD at non-zero quark-number density*, *Phys. Rev.* **D64** (2001) 094505, [[hep-lat/0105026](#)].
- [11] D. T. Son, *Superconductivity by long-range color magnetic interaction in high-density quark matter*, *Phys. Rev.* **D59** (1999) 094019, [[hep-ph/9812287](#)].
- [12] T. Schäfer, *QCD and the eta’ mass: Instantons or confinement?*, *Phys. Rev.* **D67** (2003) 074502, [[hep-lat/0211035](#)].
- [13] T. Kanazawa, T. Wettig, and N. Yamamoto, *Chiral Lagrangian and spectral sum rules for dense two- color QCD*, *JHEP* **08** (2009) 003, [[arXiv:0906.3579](#)].
- [14] C. W. J. Beenakker, *Applications of random matrix theory to condensed matter and optical physics*, [arXiv:0904.1432](#). To appear in *The Oxford Handbook of Random Matrix Theory*, Oxford University Press 2011, editors G. Akemann, J. Baik, and P. Di Francesco.
- [15] A. Zabrodin, *Random matrices and Laplacian growth*, [arXiv:0907.4929](#). To appear in *The Oxford Handbook of Random Matrix Theory*, Oxford University Press 2011, editors G. Akemann, J. Baik, and P. Di Francesco.
- [16] J. P. Bouchaud and M. Potters, *Financial Applications of Random Matrix Theory: a short*

- review, [arXiv:0910.1205](https://arxiv.org/abs/0910.1205). To appear in The Oxford Handbook of Random Matrix Theory, Oxford University Press 2011, editors G. Akemann, J. Baik, and P. Di Francesco.
- [17] J. J. M. Verbaarschot, *Handbook Article on Applications of Random Matrix Theory to QCD*, [arXiv:0910.4134](https://arxiv.org/abs/0910.4134). To appear in The Oxford Handbook of Random Matrix Theory, Oxford University Press 2011, editors G. Akemann, J. Baik, and P. Di Francesco.
- [18] Y. V. Fyodorov and D. V. Savin, *Resonance Scattering of Waves in Chaotic Systems*, [arXiv:1003.0702](https://arxiv.org/abs/1003.0702). To appear in The Oxford Handbook of Random Matrix Theory, Oxford University Press 2011, editors G. Akemann, J. Baik, and P. Di Francesco.
- [19] P. L. Ferrari and H. Spohn, *Random Growth Models*, [arXiv:1003.0881](https://arxiv.org/abs/1003.0881). To appear in The Oxford Handbook of Random Matrix Theory, Oxford University Press 2011, editors G. Akemann, J. Baik, and P. Di Francesco.
- [20] S. N. Majumdar, *Extreme Eigenvalues of Wishart Matrices: Application to Entangled Bipartite System*, [arXiv:1005.4515](https://arxiv.org/abs/1005.4515). To appear in The Oxford Handbook of Random Matrix Theory, Oxford University Press 2011, editors G. Akemann, J. Baik, and P. Di Francesco.
- [21] P. Zinn-Justin and J. B. Zuber, *Knot theory and matrix integrals*, [arXiv:1006.1812](https://arxiv.org/abs/1006.1812). To appear in The Oxford Handbook of Random Matrix Theory, Oxford University Press 2011, editors G. Akemann, J. Baik, and P. Di Francesco.
- [22] E. V. Shuryak and J. J. M. Verbaarschot, *Random matrix theory and spectral sum rules for the Dirac operator in QCD*, *Nucl. Phys.* **A560** (1993) 306–320, [[hep-th/9212088](https://arxiv.org/abs/hep-th/9212088)].
- [23] J. J. M. Verbaarschot and T. Wettig, *Random matrix theory and chiral symmetry in QCD*, *Ann. Rev. Nucl. Part. Sci.* **50** (2000) 343–410, [[hep-ph/0003017](https://arxiv.org/abs/hep-ph/0003017)].
- [24] G. Akemann, *Matrix models and QCD with chemical potential*, *Int. J. Mod. Phys.* **A22** (2007) 1077–1122, [[hep-th/0701175](https://arxiv.org/abs/hep-th/0701175)].
- [25] M. A. Stephanov, *Random matrix model of QCD at finite density and the nature of the quenched limit*, *Phys. Rev. Lett.* **76** (1996) 4472–4475, [[hep-lat/9604003](https://arxiv.org/abs/hep-lat/9604003)].
- [26] J. C. Osborn, *Universal results from an alternate random matrix model for QCD with a baryon chemical potential*, *Phys. Rev. Lett.* **93** (2004) 222001, [[hep-th/0403131](https://arxiv.org/abs/hep-th/0403131)].
- [27] G. Akemann, J. C. Osborn, K. Splittorff, and J. J. M. Verbaarschot, *Unquenched QCD Dirac operator spectra at nonzero baryon chemical potential*, *Nucl. Phys.* **B712** (2005) 287–324, [[hep-th/0411030](https://arxiv.org/abs/hep-th/0411030)].
- [28] G. Akemann, *The complex Laguerre symplectic ensemble of non-Hermitian matrices*, *Nucl. Phys.* **B730** (2005) 253–299, [[hep-th/0507156](https://arxiv.org/abs/hep-th/0507156)].
- [29] G. Akemann and F. Basile, *Massive partition functions and complex eigenvalue correlations in Matrix Models with symplectic symmetry*, *Nucl. Phys.* **B766** (2007) 150–177, [[math-ph/0606060](https://arxiv.org/abs/math-ph/0606060)].
- [30] G. Akemann, M. J. Phillips, and H. J. Sommers, *Characteristic polynomials in real Ginibre ensembles*, *J. Phys.* **A42** (2009) 012001, [[arXiv:0810.1458](https://arxiv.org/abs/0810.1458)].
- [31] A. M. Halasz, J. C. Osborn, and J. J. M. Verbaarschot, *Random matrix triality at nonzero chemical potential*, *Phys. Rev.* **D56** (1997) 7059–7062, [[hep-lat/9704007](https://arxiv.org/abs/hep-lat/9704007)].
- [32] J. Gasser and H. Leutwyler, *Thermodynamics of Chiral Symmetry*, *Phys. Lett.* **B188** (1987) 477.
- [33] T. Kanazawa, T. Wettig, and N. Yamamoto, *Chiral random matrix theory for two-color QCD*

- at high density, *Phys. Rev.* **D81** (2010) 081701, [[arXiv:0912.4999](#)].
- [34] G. Akemann, M. J. Phillips, and H. J. Sommers, *The chiral Gaussian two-matrix ensemble of real asymmetric matrices*, *J. Phys.* **A43** (2010) 085211, [[arXiv:0911.1276](#)].
- [35] Y. V. Fyodorov, B. A. Khoruzhenko, and H.-J. Sommers, *Almost-Hermitian Random Matrices: Eigenvalue Density in the Complex Plane*, *Phys. Lett.* **A226** (1997) 46–52, [[cond-mat/9606173](#)].
- [36] Y. V. Fyodorov, B. A. Khoruzhenko, and H.-J. Sommers, *Almost Hermitian Random Matrices: Crossover from Wigner- Dyson to Ginibre Eigenvalue Statistics*, *Phys. Rev. Lett.* **79** (1997) 557–560, [[cond-mat/9703152](#)].
- [37] G. Akemann, M. Kieburg, and M. J. Phillips, *Skew-orthogonal Laguerre polynomials for chiral real asymmetric random matrices*, *J. Phys.* **A43** (2010) 375207, [[arXiv:1005.2983](#)].
- [38] B. Klein, D. Toublan, and J. Verbaarschot, *Diquark and pion condensation in random matrix models for two color QCD*, *Phys.Rev.* **D72** (2005) 015007, [[hep-ph/0405180](#)].
- [39] J. C. Osborn, K. Splittorff, and J. J. M. Verbaarschot, *Chiral symmetry breaking and the Dirac spectrum at nonzero chemical potential*, *Phys. Rev. Lett.* **94** (2005) 202001, [[hep-th/0501210](#)].
- [40] J. C. Osborn, K. Splittorff, and J. J. M. Verbaarschot, *Chiral Condensate at Nonzero Chemical Potential in the Microscopic Limit of QCD*, *Phys. Rev.* **D78** (2008) 065029, [[arXiv:0805.1303](#)].
- [41] J. J. M. Verbaarschot, *The Spectrum of the Dirac operator near zero virtuality for  $N_c = 2$  and chiral random matrix theory*, *Nucl. Phys.* **B426** (1994) 559–574, [[hep-th/9401092](#)].
- [42] A. M. Halasz and J. J. M. Verbaarschot, *Effective Lagrangians and chiral random matrix theory*, *Phys. Rev.* **D52** (1995) 2563–2573, [[hep-th/9502096](#)].
- [43] T. Kanazawa, T. Wettig, and N. Yamamoto, *Chiral Lagrangian and spectral sum rules for two-color QCD at high density*, *PoS (LAT2009)* (2009) 195, [[arXiv:0910.2300](#)].
- [44] K. Splittorff and J. J. M. Verbaarschot, *Lessons from Random Matrix Theory for QCD at Finite Density*, [arXiv:0809.4503](#).
- [45] J. C. Osborn, K. Splittorff, and J. J. M. Verbaarschot, *Phase Diagram of the Dirac Spectrum at Nonzero Chemical Potential*, *Phys. Rev.* **D78** (2008) 105006, [[arXiv:0807.4584](#)].
- [46] K. Splittorff and J. J. M. Verbaarschot, *Phase of the Fermion Determinant at Nonzero Chemical Potential*, *Phys. Rev. Lett.* **98** (2007) 031601, [[hep-lat/0609076](#)].
- [47] K. Splittorff and J. J. M. Verbaarschot, *The QCD sign problem for small chemical potential*, *Phys. Rev.* **D75** (2007) 116003, [[hep-lat/0702011](#)].
- [48] K. Splittorff, *The sign problem in the epsilon-regime of QCD*, *PoS LAT2006* (2006) 023, [[hep-lat/0610072](#)].
- [49] G. Akemann and G. Vernizzi, *Characteristic polynomials of complex random matrix models*, *Nucl. Phys.* **B660** (2003) 532–556, [[hep-th/0212051](#)].
- [50] J. C. R. Bloch and T. Wettig, *Random matrix analysis of the QCD sign problem for general topology*, *JHEP* **03** (2009) 100, [[arXiv:0812.0324](#)].
- [51] I. S. Gradshteyn and I. M. Ryzhik, *Table of Integrals, Series and Products*, . 7th Edition, Academic Press, London, UK (2007).

- [52] H. J. Sommers and W. Wieczorek, *General Eigenvalue Correlations for the Real Ginibre Ensemble*, *J. Phys.* **A41** (2008) 405003, [[arXiv:0806.2756](#)].